Numer. Math. (2017) 136:805–839
DOI 10.1007/s00211-016-0851-9

Numerische Mathematik

A residual-based a posteriori error estimator for single-phase Darcy flow in fractured porous media

Huangxin Chen[1,2] · **Shuyu Sun**[2]

Received: 21 October 2015 / Revised: 16 August 2016 / Published online: 9 December 2016

Abstract In this paper we develop an a posteriori error estimator for a mixed finite element method for single-phase Darcy flow in a two-dimensional fractured porous media. The discrete fracture model is applied to model the fractures by one-dimensional fractures in a two-dimensional domain. We consider Raviart–Thomas mixed finite element method for the approximation of the coupled Darcy flows in the fractures and the surrounding porous media. We derive a robust residual-based a posteriori error estimator for the problem with non-intersecting fractures. The reliability and efficiency of the a posteriori error estimator are established for the error measured in an energy norm. Numerical results verifying the robustness of the proposed a posteriori error estimator are given. Moreover, our numerical results indicate that the a posteriori error estimator also works well for the problem with intersecting fractures.

Huangxin Chen would like to thank the support from the King Abdullah University of Science and Technology where this work was carried out during his visit, and he also thanks the supports from the NSF of China (Grant No. 11201394), the Fundamental Research Funds for the Central Universities (Grant No. 20720150005) and Program for Prominent Young Talents in Fujian Province University. The work of Shuyu Sun was supported by King Abdullah University of Science and Technology (KAUST) through the Grant BAS/1/1351-01-01.

✉ Shuyu Sun
shuyu.sun@kaust.edu.sa

Huangxin Chen
chx@xmu.edu.cn

1 School of Mathematical Sciences and Fujian Provincial Key Laboratory on Mathematical Modeling and High Performance Scientific Computing, Xiamen University, Xiamen, Fujian 361005, China

2 Computational Transport Phenomena Laboratory, Division of Physical Science and Engineering, King Abdullah University of Science and Technology, Thuwal 23955-6900, Kingdom of Saudi Arabia

Mathematics Subject Classification 65N12 · 65N15 · 65N30

1 Introduction

Modeling and simulation of flows in subsurface fractured porous media are of great interest in many of the environmental and energy problems [17,20,38], such as petroleum reservoir engineering [32]. Various conceptual models have been established to describe flows in fractured porous media. The main models include the dual-porosity model and the discrete fracture model [7,14,19,24,34,36,43,44].

The classical dual-porosity model [7,43] assumes that the fractures are interconnected with higher permeability than that in the surrounding porous media. The global flow through the fracture network is described as an effective porous continuum, and the surrounding porous media behaves as sink or source to the fracture network. An empirical matrix-fracture transfer function is used to describe the exchange between the fractures and the surrounding porous media. The accuracy of this type of model depends on the description of the transfer functions. Some improvements were achieved by the multiple interacting continua method [34] and the multiporosity model [44]. In the discrete fracture model (DFM), the geometrical structure of the fractures is discretely resolved within the model. In the classical DFM models, the numerical model is chosen such that the fractures are also resolved by the grid. The fractures can be modeled with equidimensional discretization approach [24], which requires quite a large number of degrees of freedom (DOFs). Modeling the fractures by $(d-1)$-dimensional fractures in a d-dimensional domain is an alternative approach [8,33]. This simplification improves the computational efficiency considerably and the DFM discussed in this paper refers to this approach.

There are two types of fractures: fractures sometimes called conductors which are much more permeable than that in the surrounding porous media and those usually called barriers are less permeable than that in the surrounding porous media. In the porous media with more permeable fractures the fluid has a tendency to flow into the fractures and the normal component of the velocity is not continuous across the fracture interface. In the porous media with lower permeable fractures, the fluid tends to avoid the fractures and the pressure is not continuous across the fracture interface. For both types of fractures, the reduced models have been addressed for single-phase Darcy flow [5,22,31] where the fracture flow equations and the proper interface conditions across the fracture have been identified.

Various numerical methods based on the DFM have been used to simulate flow in fractured porous media, such as finite difference methods, finite volume methods and finite element methods (cf. [28] and the references therein). For most engineering problems, the fractures are usually much more permeable than that in the surrounding porous media and the pressure is continuous across the fracture interface. Based on the assumption of continuity of pressure across the fracture interface, the cross-flow equilibrium (CFE) concept was used in the DFM [27,45] to model flow in fractured porous media. However, the CFE assumption requires that the grids next to fractures should be small enough so that the assumption of continuity of pressure is accurate. In this paper we utilize the reduced model developed in [31] which can model both

types of fractures and allows continuity or discontinuity of pressure across the fracture interface. This reduced model alleviates the grid size constraint on the porous media near the fractures.

In order to improve the quality of numerical approximation of most finite element solutions, particularly under the presence of singularities of the solution, one frequently utilizes a suitable adaptive finite element method based on a posteriori error estimator. The adaptive finite element method based on a posteriori error estimates have been well established for second-order elliptic problems (cf. [3,42]), among which several kinds of a posteriori error estimators for Raviart–Thomas mixed finite element approximation have been studied for second-order elliptic problems (cf. [4,10,13,15,29,30]). Residual-based a posteriori error estimators for Darcy flow were obtained in [1] based on finite volume approximation and in [9,39] based on a stabilized augmented discontinuous Galerkin formulation. To our best knowledge, no a posteriori error estimates for finite element approximations of the coupled Darcy flows based on the reduced model [31] in the fractured porous media have been studied in the literature so far.

The objective of this paper is to establish a robust residual-based a posteriori error estimator for the coupled Darcy flows in fractured porous media based on Raviart–Thomas mixed finite element approximation. The analysis can be extended to the problem with more non-intersecting fractures. In [16], we have applied the adaptive mixed finite element method for the simulation of Darcy flow in the fractured porous media and developed an efficient upscaling algorithm to compute the effective permeability of the fractured porous media. The a posteriori error estimates used in [16] are derived and proved with full details in this paper. For the problem with non-intersecting fractures, we focus the analysis on the problem with single fracture in the porous media in the two-dimensional case to avoid technical difficulties. For the two and three dimensional problem with intersecting fractures, there will be more complex coupling conditions at the intersection points/curves, and the difficulty of designing the adaptive algorithm lies in the strict error estimate for the system with more complex coupling conditions. The effective coupling conditions at the intersection points between fractures for the two dimensional case have been introduced in [21,23]. However, the three dimensional case needs further modeling of coupling conditions at the intersection curves. This also deserves our future study. In the following, we employ the local approximation properties of the Scott–Zhang interpolation operator, the partial continuous *inf–sup* condition and $H(\mathrm{div})$-conforming interpolation operator (cf. [11,18]) to derive a reliable residual-based a posteriori error estimator. Here partial continuous *inf–sup* condition refers to an intermediate *inf–sup* inequality which is obtained in the proof of full continuous *inf–sup* condition. This technique refers to the similar idea used in [6]. The standard localization technique based on element bubble function and edge bubble function is used to show the efficiency of the a posteriori error estimator. Proper interface conditions across the fracture interface play an important role in the analysis, which allows us to relate the one-dimensional Darcy flow in the fracture with the two-dimensional Darcy flow in the surrounding porous media. In the numerical experiments, we test several examples in two dimensions. The case with intersecting fractures is also tested. The a posteriori error estimator derived from the problem with non-intersecting fractures can also be implemented to test the problem with intersecting fractures. The robustness of the a posteriori error estimator is

observed for the problems with non-intersecting fractures and with intersecting ones. We find that the convergence of the adaptive mixed finite element method is almost optimal, i.e., the convergence rate is almost $O(N^{-s})$, where N is the number of elements and the parameter s is the optimal exponent of error decrease which depends on the regularity of the solution and the polynomial degree of approximation space.

The outline of the paper is as follows: we first introduce some notations, the reduced model of coupled Darcy flows in fractured porous media, the associated Raviart–Thomas mixed finite element approximation, the a posteriori error estimator and main results in the next section. Sections 3 and 4 are devoted to the proofs of reliability and efficiency of the a posteriori error estimator respectively. In Sect. 5, we give some numerical results for the problems with non-intersecting or intersecting fractures. Finally we provide conclusional remarks in Sect. 6.

2 The model and main results

In this section, we begin with description of the reduced model of coupled Darcy flows in the fractured porous media. Secondly, we introduce the corresponding weak formulation and the Raviart–Thomas mixed finite element method for the reduced model. Then we define the associated a posteriori error estimators and give the main results.

2.1 Description of the model

Given a bounded and simply connected domain $\Omega \in \mathbb{R}^2$ with Lipschitz continuous boundary, the single-phase flow in the porous media domain Ω governed by a mass conservation equation and Darcy's law can be described as follows:

$$\nabla \cdot \boldsymbol{u} = q \quad \text{in } \Omega, \tag{2.1a}$$

$$\boldsymbol{u} = -\boldsymbol{K}\nabla p \quad \text{in } \Omega, \tag{2.1b}$$

$$p = g^D \quad \text{on } \Gamma^D, \tag{2.1c}$$

$$\boldsymbol{u} \cdot \boldsymbol{n}_\Gamma = g^N \quad \text{on } \partial\Omega \backslash \Gamma^D, \tag{2.1d}$$

where Γ^D is Dirichlet boundary and the remaining part $\partial\Omega\backslash\Gamma^D$ is Neumann boundary. Here we denote by p the pressure, $\boldsymbol{u}$ the Darcy velocity, $\boldsymbol{K}$ the permeability tensor, q the source term, g^D the given pressure on Γ^D, g^N the given normal component of Darcy velocity on $\partial\Omega\backslash\Gamma^D$, and $\boldsymbol{n}_\Gamma$ the unit outward normal to $\partial\Omega$.

For simplicity, we assume that there is a single fracture Ω_f in the porous media and the domain Ω is separated into three connected subdomains Ω_1, Ω_2 and Ω_f as shown in the left graph of Fig. 1 such that $\Omega_1 \cap \Omega_2 = \emptyset$. The fracture domain Ω_f is assumed to be $\Omega_f = \{x \in \Omega : x = s + t\boldsymbol{n},\ s \in \gamma \text{ and } t \in (-\frac{d(s)}{2}, \frac{d(s)}{2})\}$, where γ is a one-dimensional polygonal line, $\boldsymbol{n} = \boldsymbol{n}_1 = -\boldsymbol{n}_2$ is the unit normal vector to γ, $\boldsymbol{n}_i|_{i=1,2}$ is the unit normal on $\partial\Omega_i \cap \partial\Omega_f$ outwards with respect to Ω_i, and $d(s)$ denotes the thickness of fracture at the point $s \in \gamma$. Throughout the paper, we assume that the permeability tensor is isotropic and positive definite in the porous media subdomains

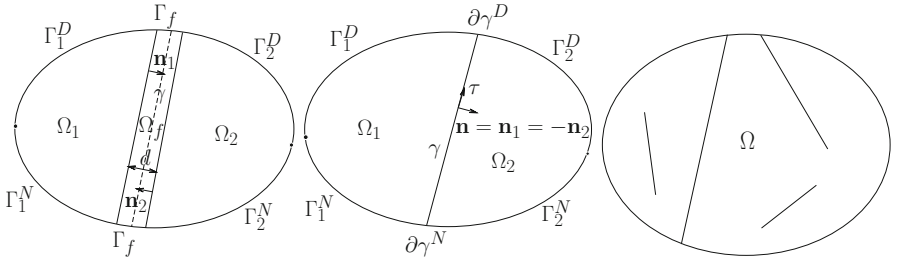

Fig. 1 *Left* The domain Ω with a single fracture Ω_f. *Middle* The subdomains Ω_1, Ω_2 and the reduced fracture γ. *Right* The domain Ω and more reduced fractures non-immersed, immersed or partially immersed in Ω

Ω_1, Ω_2, and it is denoted by $\boldsymbol{K}_i$ in Ω_i for $i = 1, 2$. The permeability tensor in Ω_f is denoted by $\boldsymbol{K}_f$, and we assume

$$\boldsymbol{K}_f = \begin{pmatrix} \boldsymbol{K}_{f,\boldsymbol{\tau}} & 0 \\ 0 & \boldsymbol{K}_{f,\boldsymbol{n}} \end{pmatrix},$$

where $\boldsymbol{K}_{f,\boldsymbol{\tau}} = (\boldsymbol{K}_f\boldsymbol{\tau}, \boldsymbol{\tau})$ and $\boldsymbol{K}_{f,\boldsymbol{n}} = (\boldsymbol{K}_f\boldsymbol{n}, \boldsymbol{n})$. Here $\boldsymbol{\tau}$ is the unit tangential vector to γ. In this paper we always assume $(\boldsymbol{K}_f\boldsymbol{\tau}, \boldsymbol{n}) = 0$ which can be nonzero in more general case but the analysis of the reduced model for flow in the fractured porous media then becomes more intricate. If the Darcy flow is solved in Ω_f as a two-dimensional problem, the grid in Ω_f should be sufficiently fine and this requires a large number of computation resources. We will utilize the reduced model proposed in [31] based on the DFM to describe the Darcy flow in Ω_f as a lower dimensional problem.

Now we give some notations which will be used in the sequel. We denote by $\nabla_{\boldsymbol{\tau}}$ and $\nabla_{\boldsymbol{\tau}}\cdot$ the tangential gradient and divergence operators along γ, and $\nabla_{\boldsymbol{n}}$ and $\nabla_{\boldsymbol{n}}\cdot$ the normal gradient and divergence operators along γ. Let $\Gamma_f = \partial\Omega_f \cap \partial\Omega$, $\Gamma^N = \partial\Omega\backslash(\Gamma_f \cup \Gamma^D)$. We denote by Γ_f^D the Dirichlet boundary and Γ_f^N the Neumann boundary on $\partial\Omega_f \cap \partial\Omega$ and assume $\overline{\Gamma_f^D} \cap \overline{\Gamma_f^N} = \emptyset$. The ends of γ are denoted by $\partial\gamma^D = \gamma \cap \Gamma_f^D$ and $\partial\gamma^N = \gamma \cap \Gamma_f^N$. For the domain shown in the middle graph of Fig. 1 for the reduced model, we denote by Γ_i^D and Γ_i^N the Dirichlet and Neumann boundary respectively in the subdomain Ω_i, $i = 1, 2$. Let $\boldsymbol{u}_i$, p_i, q_i be the restrictions of $\boldsymbol{u}$, p, q in Ω_i for $i = 1, 2$, f, and $p_i^D = p^D|_{\Gamma_i^D}$, $g_i^N = g^N|_{\Gamma_i^N}$ for $i = 1, 2$. We denote by $\{\cdot\}_\gamma$ the average of a quantity on γ such that $\{\psi\}_\gamma = \frac{1}{2}(\psi_1|_\gamma + \psi_2|_\gamma)$ and $[\![\psi]\!]_\gamma$ the jump of a quantity across γ such that $[\![\psi]\!]_\gamma = \psi_1|_\gamma - \psi_2|_\gamma$, where $\psi_i|_{i=1,2}$ is a function defined in Ω_i with well defined trace on γ. Next we define several quantities to be used in the reduced model:

$$\widehat{\boldsymbol{u}}_\gamma = \int_{-\frac{d(s)}{2}}^{\frac{d(s)}{2}} (\boldsymbol{u}_f(s,t)\cdot\boldsymbol{\tau}(s))\boldsymbol{\tau}(s)dt, \quad \widehat{p}_\gamma = \frac{1}{d(s)}\int_{-\frac{d(s)}{2}}^{\frac{d(s)}{2}} p_f(s,t)dt,$$

$$\widehat{q}_\gamma = \int_{-\frac{d(s)}{2}}^{\frac{d(s)}{2}} q_f(s,t)dt, \quad \widehat{\boldsymbol{u}}_\gamma^{\boldsymbol{n}} = \int_{-\frac{d(s)}{2}}^{\frac{d(s)}{2}} (\boldsymbol{u}_f(s,t)\cdot\boldsymbol{n}(s))\boldsymbol{n}(s)dt,$$
$$\widehat{g}_\gamma^N = \int_{\Gamma_f^N} g^N(s,t)dt, \quad \widehat{g}_\gamma^D = \frac{1}{d(s)}\int_{\Gamma_f^D} g^D(s,t)dt.$$

By averaging the conservation equation (2.1a) and the Darcy's law (2.1b) over cross-section of the fracture, the reduced model within the domain in the middle graph of Fig. 1 reads as follows (cf. [31]):

$$\nabla\cdot\boldsymbol{u}_i = q_i \quad \text{in } \Omega_i,\ i=1,2, \tag{2.2a}$$
$$\boldsymbol{u}_i = -\boldsymbol{K}_i\nabla p_i \quad \text{in } \Omega_i,\ i=1,2, \tag{2.2b}$$
$$\nabla_{\boldsymbol{\tau}}\cdot\widehat{\boldsymbol{u}}_\gamma = \widehat{q}_\gamma + [\![\boldsymbol{u}\cdot\boldsymbol{n}]\!]_\gamma, \quad \text{on } \gamma, \tag{2.2c}$$
$$\widehat{\eta}_\gamma\widehat{\boldsymbol{u}}_\gamma + \nabla_{\boldsymbol{\tau}}\widehat{p}_\gamma = 0 \quad \text{on } \gamma, \tag{2.2d}$$
$$\xi_\gamma\eta_\gamma[\![\boldsymbol{u}\cdot\boldsymbol{n}]\!]_\gamma = \{p\}_\gamma - \widehat{p}_\gamma \quad \text{on } \gamma, \tag{2.2e}$$
$$\eta_\gamma\{\boldsymbol{u}\cdot\boldsymbol{n}\}_\gamma = [\![p]\!]_\gamma, \quad \text{on } \gamma, \tag{2.2f}$$
$$p_i = g_i^D \quad \text{on } \Gamma_i^D,\ i=1,2, \tag{2.2g}$$
$$\boldsymbol{u}_i\cdot\boldsymbol{n}_\Gamma = g_i^N \quad \text{on } \Gamma_i^N,\ i=1,2, \tag{2.2h}$$
$$\widehat{p}_\gamma = \widehat{g}_\gamma^D \quad \text{on } \partial\gamma^D, \tag{2.2i}$$
$$\widehat{\boldsymbol{u}}_\gamma\cdot\boldsymbol{n}_\Gamma = \widehat{g}_\gamma^N \quad \text{on } \partial\gamma^N, \tag{2.2j}$$

where (2.2e) and (2.2f) are interface conditions coupling the one-dimensional problem (2.2c) and (2.2d) in the reduced fracture and the two-dimensional problems (2.2a) and (2.2b) in the surrounding porous media. The parameters in (2.2e) and (2.2f) are defined as

$$\widehat{\eta}_\gamma = \frac{1}{d(s)\boldsymbol{K}_{f,\boldsymbol{\tau}}}, \quad \eta_\gamma = \frac{d(s)}{\boldsymbol{K}_{f,\boldsymbol{n}}} \quad \text{and} \quad \xi_\gamma = \frac{2\xi-1}{4},\ \xi > \frac{1}{2}.$$

Remark 1 In the sequel we always assume that $\widehat{\eta}_\gamma$, η_γ and the eigenvalues of $\boldsymbol{K}_i|_{i=1,2}$ are bounded below and above as in [31]. $\widehat{\boldsymbol{u}}_\gamma^{\boldsymbol{n}}$ can be directly obtained by $\widehat{\boldsymbol{u}}_\gamma^{\boldsymbol{n}} = -\boldsymbol{K}_{f,\boldsymbol{n}}(p_2|_\gamma - p_1|_\gamma)\boldsymbol{n}$. When the fractures are more permeable than that in the surrounding porous media, the Neumann boundary condition on $\partial\gamma^N$, which is immersed in the porous media, can be considered as $\widehat{\boldsymbol{u}}_\gamma\cdot\boldsymbol{\tau}|_{\partial\gamma^N} = 0$. Therefore, in such a case the reduced model (2.2) can be extended to the problem with more reduced non-intersecting fractures as described in the right graph of Fig. 1.

2.2 Weak formulation and mixed finite element approximation of the reduced model

Throughout this paper, we use the standard notations and definitions for Sobolev spaces (cf. [2]). For any $D\subset\overline{\Omega}$, any scalar functions ψ and ϕ, or vector functions $\boldsymbol{\psi}$ and $\boldsymbol{\phi}$, we define

$$(\psi,\phi)_D=\int_D\psi\phi,\quad(\boldsymbol{\psi},\boldsymbol{\phi})_D=\int_D\boldsymbol{\psi}\cdot\boldsymbol{\phi},\qquad\text{if }\dim(D)\geq 1.$$

We use the notation $\|\cdot\|_{0,D}$ to denote the L^2-norm on D. If $D=\mathcal{Z}$, where $\mathcal{Z}\subset\overline{\Omega}$ is a set of vertices, we define $(\psi,\phi)_{\mathcal{Z}}=\sum_{z\in\mathcal{Z}}\psi(z)\phi(z)$. In order to introduce the weak formulation of the reduced model (2.2), we define the sets

$$\begin{aligned}\boldsymbol{U}_i^{g_i^N}&=\{\boldsymbol{v}_i\in H(\mathrm{div},\Omega_i):\ \boldsymbol{v}_i\cdot\boldsymbol{n}_\Gamma=g_i^N\text{ on }\Gamma_i^N,\ \boldsymbol{v}_i\cdot\boldsymbol{n}_i\in L^2(\gamma)\},\ i=1,2,\\ \boldsymbol{U}_\gamma^{\widehat{g}_\gamma^N}&=\{\widehat{\boldsymbol{v}}_\gamma\in[L^2(\gamma)]^2:\ \widehat{\boldsymbol{v}}_\gamma\cdot\boldsymbol{n}=0,\ \nabla_{\boldsymbol{\tau}}\cdot\widehat{\boldsymbol{v}}_\gamma\in L^2(\gamma),\ \widehat{\boldsymbol{v}}_\gamma\cdot\boldsymbol{n}_\Gamma=\widehat{g}_\gamma^N\}.\end{aligned}$$

In addition, we let $g^D=(g_1^D,g_2^D,\widehat{g}_\gamma^D)$, $g^N=(g_1^N,g_2^N,\widehat{g}_\gamma^N)$, $Q_1=L^2(\Omega_1)$, $Q_2=L^2(\Omega_2)$, $Q_\gamma=L^2(\gamma)$ and define

$$\boldsymbol{U}^{g^N}=\boldsymbol{U}_1^{g_1^N}\times\boldsymbol{U}_2^{g_2^N}\times\boldsymbol{U}_\gamma^{\widehat{g}_\gamma^N}\quad\text{and}\quad Q=Q_1\times Q_2\times Q_\gamma$$

endowed with the product norms

$$\begin{aligned}\|\boldsymbol{v}^*\|_{\boldsymbol{U}}^2&=\sum_{i=1}^2\left(\|\boldsymbol{v}_i\|_{0,\Omega_i}^2+\|\nabla\cdot\boldsymbol{v}_i\|_{0,\Omega_i}^2\right)+\sum_{i=1}^2\|\boldsymbol{v}_i\cdot\boldsymbol{n}\|_{0,\gamma}^2+\|\widehat{\boldsymbol{v}}_\gamma\|_{0,\gamma}^2+\|\nabla_{\boldsymbol{\tau}}\cdot\widehat{\boldsymbol{v}}_\gamma\|_{0,\gamma}^2,\\ \|r^*\|_Q^2&=\sum_{i=1}^2\|r_i\|_{0,\Omega_i}^2+\|\widehat{r}_\gamma\|_{0,\gamma}^2\end{aligned}$$

for all $\boldsymbol{v}^*=(\boldsymbol{v}_1,\boldsymbol{v}_2,\widehat{\boldsymbol{v}}_\gamma)\in\boldsymbol{U}^{g^N}$ and $r^*=(r_1,r_2,\widehat{r}_\gamma)\in Q$.

Since the two ends of γ may be intersected with Γ_i^D or Γ_i^N, $i=1,2$, we consider the case that one end $\partial\gamma^N$ of γ is intersected with Γ_1^N and Γ_2^N, and another end $\partial\gamma^D$ of γ is intersected with Γ_1^D and Γ_2^D (cf. middle graph in Fig. 1). In the following we always assume $\Gamma_i^D|_{i=1,2}\neq\emptyset$, $\Gamma_i^N|_{i=1,2}\neq\emptyset$, $\partial\gamma^D\neq\emptyset$, $\partial\gamma^N\neq\emptyset$ and $g^N=0$ for simplicity. Extension to non-homogeneous Neumann boundary condition is straightforward.

Now the weak formulation of the reduced model (2.2) can be written as follows: Find $(\boldsymbol{u}^*,p^*)\in\boldsymbol{U}^0\times Q$ such that

$$a(\boldsymbol{u}^*,\boldsymbol{v}^*)-b(\boldsymbol{v}^*,p^*)=G(g^D,\boldsymbol{v}^*)\quad\forall\,\boldsymbol{v}^*\in\boldsymbol{U}^0,\tag{2.3a}$$

$$b(\boldsymbol{u}^*,r^*)=L(q^*,r^*)\quad\forall\,r^*\in Q,\tag{2.3b}$$

where

$$\begin{aligned}a(\boldsymbol{u}^*,\boldsymbol{v}^*)=&\sum_{i=1}^2(\boldsymbol{K}_i^{-1}\boldsymbol{u}_i,\boldsymbol{v}_i)_{\Omega_i}+(\widehat{\eta}_\gamma\widehat{\boldsymbol{u}}_\gamma,\widehat{\boldsymbol{v}}_\gamma)_\gamma\\&+(\eta_\gamma\{\boldsymbol{u}\cdot\boldsymbol{n}\}_\gamma,\{\boldsymbol{v}\cdot\boldsymbol{n}\}_\gamma)_\gamma+(\xi_\gamma\eta_\gamma[\![\boldsymbol{u}\cdot\boldsymbol{n}]\!]_\gamma,[\![\boldsymbol{v}\cdot\boldsymbol{n}]\!]_\gamma)_\gamma,\end{aligned}$$

$$b(\boldsymbol{u}^*, r^*) = \sum_{i=1}^{2} (\nabla \cdot \boldsymbol{u}_i, r_i)_{\Omega_i} + (\nabla_{\boldsymbol{\tau}} \cdot \widehat{\boldsymbol{u}}_\gamma, \widehat{r}_\gamma)_\gamma - ([\![\boldsymbol{u} \cdot \boldsymbol{n}]\!]_\gamma, \widehat{r}_\gamma)_\gamma,$$

$$G(g^D, \boldsymbol{v}^*) = -\sum_{i=1}^{2} \left(g_i^D, \boldsymbol{v}_i \cdot \boldsymbol{n}_\Gamma\right)_{\Gamma_i^D} - \left(\widehat{g}_\gamma^D, \widehat{\boldsymbol{v}}_\gamma \cdot \boldsymbol{n}_\Gamma\right)_{\partial\gamma^D},$$

$$L(q^*, r^*) = \sum_{i=1}^{2} (q_i, r_i)_{\Omega_i} + \left(\widehat{q}_\gamma, \widehat{r}_\gamma\right)_\gamma.$$

The weak formulation admits a unique solution (cf. [31]) since that the bilinear form $a(\cdot,\cdot)$ is continuous and $\widetilde{\boldsymbol{U}}^0$-elliptic, i.e.,

$$\exists\, \alpha > 0, \text{ such that } a(\boldsymbol{v}^*, \boldsymbol{v}^*) \geq \alpha \|\boldsymbol{v}^*\|_{\boldsymbol{U}} \quad \forall\, \boldsymbol{v}^* \in \widetilde{\boldsymbol{U}}^0,$$

where $\widetilde{\boldsymbol{U}}^0 = \{\boldsymbol{v}^* \in \boldsymbol{U}^0 : \ b(\boldsymbol{v}^*, r^*) = 0 \ \ \forall\, r^* \in Q\}$, and the bilinear form $b(\cdot,\cdot)$ is continuous and satisfies the *inf–sup* condition:

$$\exists\, \beta > 0, \ \forall\, r^* \in Q, \ \exists\, \boldsymbol{v}^* \in \boldsymbol{U}^0, \ \boldsymbol{v}^* \neq 0 \text{ such that } b(\boldsymbol{v}^*, r^*) \geq \beta \|\boldsymbol{v}^*\|_{\boldsymbol{U}} \|r^*\|_Q.$$

Next we introduce the Raviart–Thomas mixed finite element approximation of the weak formulation (2.3). Let $\mathcal{T}_h^i$ be a conforming, shape-regular simplicial triangulation of Ω_i, $i = 1, 2$, and $\mathcal{T}_h^\gamma$ be the finite element partition of γ. We assume that the partitions $\mathcal{T}_h^1$, $\mathcal{T}_h^2$ and $\mathcal{T}_h^\gamma$ are matching at the interface γ. We now define the finite element subspaces of $\boldsymbol{U}^0$ and Q. Let $\mathrm{RT}_k = [\mathbb{P}_k]^2 \oplus \boldsymbol{x}\mathbb{P}_k$ where $\mathbb{P}_k$ is the polynomial space of degree $k \geq 0$. Here RT_k is the well-known Raviart–Thomas finite element space of order k. We define

$$\boldsymbol{U}_h^0 = \boldsymbol{U}_{1,h}^0 \times \boldsymbol{U}_{2,h}^0 \times \boldsymbol{U}_{\gamma,h}^0 \quad \text{and} \quad Q_h = Q_{1,h} \times Q_{2,h} \times Q_{\gamma,h},$$

where

$$\boldsymbol{U}_{i,h}^0 = \{\boldsymbol{v}_i \in \boldsymbol{U}_i^0 : \ \boldsymbol{v}_i|_T \in \mathrm{RT}_k(T), \ \forall\, T \in \mathcal{T}_h^i\}, \quad i = 1, 2,$$
$$Q_{i,h} = \{r_i \in Q_i : \ r_i|_T \in \mathbb{P}_k(T), \ \forall\, T \in \mathcal{T}_h^i\}, \quad i = 1, 2,$$

and

$$\boldsymbol{U}_{\gamma,h}^0 = \{\widehat{\boldsymbol{v}}_\gamma \in \boldsymbol{U}_\gamma^0 : \ \widehat{\boldsymbol{v}}_\gamma|_e \in \mathrm{RT}_k(e), \ \forall\, e \in \mathcal{T}_h^\gamma\},$$
$$Q_{\gamma,h} = \{\widehat{r}_\gamma \in Q_\gamma : \ \widehat{r}_\gamma|_e \in \mathbb{P}_k(e), \ \forall\, e \in \mathcal{T}_h^\gamma\}.$$

Using the spaces $\boldsymbol{U}_h^0 \subset \boldsymbol{U}^0$ and $Q_h \subset Q$, the discrete approximation of the weak formulation (2.3) can be written as follows: Find $(\boldsymbol{u}_h^*, p_h^*) \in \boldsymbol{U}_h^0 \times Q_h$ such that

$$a(\boldsymbol{u}_h^*, \boldsymbol{v}_h^*) - b(\boldsymbol{v}_h^*, p_h^*) = G(g^D, \boldsymbol{v}_h^*) \quad \forall\, \boldsymbol{v}_h^* = (\boldsymbol{v}_h^1, \boldsymbol{v}_h^2, \widehat{\boldsymbol{v}}_h^\gamma) \in \boldsymbol{U}_h^0, \tag{2.4a}$$

$$b(\boldsymbol{u}_h^*, r_h^*) = L(q^*, r_h^*) \quad \forall\, r_h^* = (r_h^1, r_h^2, \widehat{r}_h^{\gamma}) \in Q_h. \tag{2.4b}$$

The well-posedness of the above discrete problem holds provided that the bilinear form $a(\cdot,\cdot)$ is discrete $\widetilde{\boldsymbol{U}}^0$-elliptic and the bilinear form $b(\cdot,\cdot)$ satisfies the discrete *inf–sup* condition (cf. [11]). Indeed, the discrete $\widetilde{\boldsymbol{U}}^0$-elliptic property of $a(\cdot,\cdot)$ can be implied by the facts that $\nabla\cdot\boldsymbol{U}_{1,h}^0 \times \nabla\cdot\boldsymbol{U}_{2,h}^0 \times \nabla_{\boldsymbol{\tau}}\cdot\boldsymbol{U}_{\gamma,h}^0 \subset Q_h$ and $[\![\boldsymbol{v}_h\cdot\boldsymbol{n}]\!]_\gamma \in Q_{\gamma,h}$ for any $\boldsymbol{v}_h = (\boldsymbol{v}_h^1, \boldsymbol{v}_h^2) \in \boldsymbol{U}_{1,h}^0 \times \boldsymbol{U}_{2,h}^0$. The discrete *inf–sup* condition of $b(\cdot,\cdot)$ can be derived by the Fortin's lemma (cf. [11]) through proper interpolation operators (cf. [11,18]) from $\boldsymbol{U}^0$ into $\boldsymbol{U}_h^0$. The *a priori* error estimates for the discrete problem (2.4) have been discussed in [31].

2.3 A posteriori error estimators and main results

We begin with some notations. For $i = 1, 2$, we denote by $\mathcal{E}_h(\Omega_i)$ the set of all the edges of the triangulation $\mathcal{T}_h^i$, $\mathcal{E}_h^0(\Omega_i)$ the set of all the interior edges of the triangulation $\mathcal{T}_h^i$, $\mathcal{E}_h(\Gamma_i^D)$ the set of all boundary edges on Γ_i^D and $\mathcal{E}_h$ the set of all edges of the triangulations $\mathcal{T}_h^1 \cup \mathcal{T}_h^2$. We have assumed the partitions $\mathcal{T}_h^1$, $\mathcal{T}_h^2$ and $\mathcal{T}_h^\gamma$ are matching at γ, thus $\mathcal{T}_h^\gamma \subset \mathcal{E}_h$. Then we set $\mathcal{T}_h = \mathcal{T}_h^1 \cup \mathcal{T}_h^2$. We denote by $\mathcal{N}_h^0(\gamma)$ the set of interior vertices on $\mathcal{T}_h^\gamma$. For any $T \in \mathcal{T}_h$, let h_T be the diameter of element T. For any edge $e \in \mathcal{E}_h$, h_e stands for the diameter of e. For any interior edge $e = \partial T \cap \partial T'$ in $\mathcal{E}_h^0(\Omega_i)$, $i = 1, 2$, we denote by $[\![\psi]\!] = (\psi|_T)|_e - (\psi|_{T'})|_e$ the jump of scalar function ψ across e. For any edge $e \in \mathcal{E}_h$, we let $\boldsymbol{s}_e$ be the unit tangential vector along e and $\boldsymbol{n}_e$ be the unit normal vector along e. If no confusion is possible, we write $\boldsymbol{s}$ instead of $\boldsymbol{s}_e$. We denote by $\mathcal{P}_T$ the L^2-projection operator from $L^2(T)$ onto $\mathbb{P}_k(T)$ for any $T \in \mathcal{T}_h$. Similarly, $\mathcal{P}_e$ denotes the L^2-projection operator from $L^2(e)$ onto $\mathbb{P}_k(e)$ for any $e \in \mathcal{E}_h$. For sufficiently smooth scalar and vector functions w and $\boldsymbol{v}$, we let $\mathbf{curl}\, w = (\frac{\partial w}{\partial x_2}, -\frac{\partial w}{\partial x_1})^t$ and $\mathrm{curl}\, \boldsymbol{v} = \frac{\partial v_1}{\partial x_2} - \frac{\partial v_2}{\partial x_1}$. In order to derive robust a posteriori error estimator for the discrete problem (2.4), for $i = 1, 2$, in the sequel we assume $g_i^D \in H^1(e)$ on each $e \in \mathcal{E}_h(\Gamma_i^D)$, and the trace of p_i is $H^{1/2}(e)$ on each $e \in \mathcal{T}_h^\gamma$.

Given $(\boldsymbol{u}_h^*, p_h^*)$ the unique solution of the discrete problem (2.4), we first define for each $T \in \mathcal{T}_h^i$ the a posteriori error indicator

$$\eta_T^2 = \eta_{T,1}^2 + \eta_{T,2}^2 + \eta_{T,3}^2,$$

where $\eta_{T,1}^2 = h_T^2 \|\mathrm{curl}\,(\boldsymbol{K}_i^{-1}\boldsymbol{u}_h^i)\|_{0,T}^2$, $\eta_{T,2}^2 = \|q_i - \nabla\cdot\boldsymbol{u}_h^i\|_{0,T}^2$, $\eta_{T,3}^2 = h_T^2\|\boldsymbol{K}_i^{-1}\boldsymbol{u}_h^i + \nabla p_h^i\|_{0,T}^2$, $i = 1, 2$, and for each $e \in \mathcal{E}_h^0(\Omega_i)$ the a posteriori error indicator

$$\eta_e^2 = h_e\|[\![\boldsymbol{K}_i^{-1}\boldsymbol{u}_h^i\cdot\boldsymbol{s}]\!]\|_{0,e}^2, \quad i = 1, 2.$$

Similarly, for $e \in \mathcal{E}_h(\Gamma_i^D)$, $i = 1, 2$, we set

$$\eta_{e,\Gamma_i^D}^2 = h_e\|\boldsymbol{K}_i^{-1}\boldsymbol{u}_h^i\cdot\boldsymbol{s} + \frac{dg_i^D}{d\boldsymbol{s}}\|_{0,e}^2,$$

$$\mathrm{osc}^2_{e,1,\Gamma_i^D} = h_e \| g_i^D - \mathcal{P}_e g_i^D \|^2_{0,e},$$
$$\mathrm{osc}^2_{e,2,\Gamma_i^D} = h_e \| \frac{dg_i^D}{ds} - \frac{d\mathcal{P}_e g_i^D}{ds} \|^2_{0,e}.$$

For each $e \in \mathcal{T}_h^\gamma$, we set

$$\eta^2_{e,\gamma} = \eta^2_{e,\gamma,1} + \eta^2_{e,\gamma,2} + \eta^2_{e,\gamma,3},$$

where

$$\eta^2_{e,\gamma,1} = \sum_{i=1}^{2} h_e^2 \| (\boldsymbol{K}_i^{-1}\boldsymbol{u}_h^i + \nabla p_h^i)\cdot\boldsymbol{\tau}\|^2_{0,e} + \| \{p_h\}_\gamma - \widehat{p}_h^\gamma - \xi_\gamma \eta_\gamma [\![\boldsymbol{u}_h \cdot \boldsymbol{n}]\!]_\gamma \|^2_{0,e}$$
$$+ \| [\![p_h]\!]_\gamma - \eta_\gamma \{\boldsymbol{u}_h \cdot \boldsymbol{n}\}_\gamma \|^2_{0,e} + \sum_{i=1}^{2} \| p_h^i - \Pi_h^i p_h^i \|^2_{0,e} + \| \widehat{p}_h^\gamma - \Pi_h^\gamma \widehat{p}_h^\gamma \|^2_{0,e},$$
$$\eta^2_{e,\gamma,2} = \| \widehat{q}_\gamma - \nabla_{\boldsymbol{\tau}} \cdot \widehat{\boldsymbol{u}}_h^\gamma + [\![\boldsymbol{u}_h \cdot \boldsymbol{n}]\!]_\gamma \|^2_{0,e} \quad \text{and} \quad \eta^2_{e,\gamma,3} = h_e^2 \| (\widehat{\eta}_\gamma \widehat{\boldsymbol{u}}_h^\gamma + \nabla_{\boldsymbol{\tau}} \widehat{p}_h^\gamma)\cdot\boldsymbol{\tau}\|^2_{0,e}.$$

When the polynomial degree $k \geq 1$, $\Pi_h^i : Q_{i,h}|_\gamma \to C^0(\gamma) \cap (Q_{i,h}|_\gamma)$, $i = 1, 2$ and $\Pi_h^\gamma : Q_{\gamma,h} \to C^0(\gamma) \cap Q_{\gamma,h}$ are continuous piecewise interpolation operators defined on γ as follows: for any degree of freedom z,

$$\Pi_h^i p_h^i(z) = \begin{cases} \frac{1}{2}\left(p_h^i|_e(z) + p_h^i|_{e'}(z) \right), & z \in \mathcal{N}_h^0(\gamma), \quad z = \partial e \cap \partial e', \\ p_h^i(z), & \text{otherwise}, \end{cases} \tag{2.5}$$

and

$$\Pi_h^\gamma \widehat{p}_h^\gamma(z) = \begin{cases} \frac{1}{2}\left(\widehat{p}_h^\gamma|_e(z) + \widehat{p}_h^\gamma|_{e'}(z) \right), & z \in \mathcal{N}_h^0(\gamma), \quad z = \partial e \cap \partial e', \\ \widehat{p}_h^\gamma(z), & \text{otherwise}. \end{cases} \tag{2.6}$$

When $k = 0$, $\Pi_h^i|_{i=1,2}$ and Π_h^γ are continuous piecewise linear interpolation operators defined as above. Let $e_d \in \mathcal{T}_h^\gamma$, $\partial\gamma^D \in \partial e_d$, and $T_i^* \in \mathcal{T}_h^i$, $e_d \subset \partial T_i^*$ for $i = 1, 2$. For $\partial\gamma^D$, we set

$$\eta^2_{\partial\gamma^D} = \sum_{i=1}^{2} h_{e_d} \left(g_i^D - (p_h^i|_{T_i^*})|_{\partial\gamma^D} \right)^2 + h_{e_d} \left(\widehat{g}_\gamma^D - \widehat{p}_h^\gamma|_{\partial\gamma^D} \right)^2.$$

Then the global a posteriori error estimator is defined as

$$\eta^2 = \sum_{i=1}^{2} \left(\sum_{T\in\mathcal{T}_h^i} \eta_T^2 + \sum_{e\in\mathcal{E}_h^0(\Omega_i)} \eta_e^2 + \sum_{e\in\mathcal{E}_h(\Gamma_i^D)} \eta^2_{e,\Gamma_i^D} \right) + \sum_{e\in\mathcal{T}_h^\gamma} \eta^2_{e,\gamma} + \eta^2_{\partial\gamma^D}.$$

For any $(\boldsymbol{v}^*, r^*) \in \boldsymbol{U}^0 \times Q$, we define the mesh-dependent energy norm

$$
\begin{aligned}
|||(\boldsymbol{v}^*, r^*)|||_h^2 &= \|\boldsymbol{v}^*\|_{\boldsymbol{U}}^2 + \|r^*\|_Q^2 + \sum_{i=1}^{2} h_{e_d}\big((r_i|_{T_i^*})|_{\partial\gamma^D}\big)^2 \\
&+ h_{e_d}\big(\widehat{r}_\gamma|_{\partial\gamma^D}\big)^2 + \sum_{i=1}^{2}\sum_{z\in\mathcal{N}_h^0(\gamma)} h_z[\![r_i]\!]_z^2 + \sum_{z\in\mathcal{N}_h^0(\gamma)} h_z[\![\widehat{r}_\gamma]\!]_z^2 \\
&+ \sum_{e\in\mathcal{T}_h^\gamma}\Big(\|\{r\}_\gamma - \widehat{r}_\gamma - \xi_\gamma\eta_\gamma[\![\boldsymbol{v}\cdot\boldsymbol{n}]\!]_\gamma\|_{0,e}^2 + \|[\![r]\!]_\gamma - \eta_\gamma\{\boldsymbol{v}\cdot\boldsymbol{n}\}_\gamma\|_{0,e}^2\Big), \qquad (2.7)
\end{aligned}
$$

where $h_z = \max\{h_e : z \in \partial e,\ e \in \mathcal{T}_h^\gamma\}$, $[\![r_i]\!]_z = r_i|_e(z) - r_i|_{e'}(z)$ and $[\![\widehat{r}_\gamma]\!]_z = \widehat{r}_\gamma|_e(z) - \widehat{r}_\gamma|_{e'}(z)$ for any $z \in \mathcal{N}_h^0(\gamma)$ and $\partial e \cap \partial e' = z$. From now on, we denote by C with or without subscript a positive constant depending only on the shape regularity of the meshes and the polynomial degree. These constants can take on different values in different occurrences. If $CB \le A \le CB$, we denote $A \approx B$. We outline the main results by showing the reliability and efficiency of the a posteriori error estimator respectively in the following theorem.

Theorem 2.1 *Let $(\boldsymbol{u}^*, p^*)$ and $(\boldsymbol{u}_h^*, p_h^*)$ be the solutions of (2.3) and (2.4) respectively. Then there exist positive constants C_{rel} and C_{eff} such that*

$$
|||(\boldsymbol{u}^* - \boldsymbol{u}_h^*, p^* - p_h^*)|||_h \le C_{\mathrm{rel}}\,(\eta + \mathrm{osc}_{1,\Gamma^D}), \qquad (2.8)
$$

$$
\eta \le C_{\mathrm{eff}}\big(\,|||\,(\boldsymbol{u}^* - \boldsymbol{u}_h^*, p^* - p_h^*)\,|||_h + \mathrm{osc}_{2,\Gamma^D}\big), \qquad (2.9)
$$

where $\mathrm{osc}_{k,\Gamma^D} = \big(\sum_{i=1}^{2}\sum_{e\in\mathcal{E}_h(\Gamma_i^D)}\mathrm{osc}_{e,k,\Gamma_i^D}^2\big)^{1/2}$, $k = 1, 2$.

3 Proof of reliability estimate

In this section, we give the proof of estimate (2.8) in Theorem 2.1, which shows the reliability of the a posteriori error estimator. The proof focuses on the derivation of upper bounds for the error $\|\boldsymbol{u}^* - \boldsymbol{u}_h^*\|_{\boldsymbol{U}}$ and $\|p^* - p_h^*\|_Q$. We will apply the technique used in [6] to derive the upper bound for $\|\boldsymbol{u}^* - \boldsymbol{u}_h^*\|_{\boldsymbol{U}}$ into two steps. Firstly, we give the following preliminary estimate.

Lemma 3.1 *There exists a positive constant C such that*

$$
C\|\boldsymbol{u}^* - \boldsymbol{u}_h^*\|_{\boldsymbol{U}} \le \sup_{\substack{\boldsymbol{v}^*\in\widetilde{\boldsymbol{U}}^0\\ \boldsymbol{v}^*\neq 0}} \frac{a(\boldsymbol{u}^* - \boldsymbol{u}_h^*, \boldsymbol{v}^*)}{\|\boldsymbol{v}^*\|_{\boldsymbol{U}}} + \left(\sum_{i=1}^{2}\sum_{T\in\mathcal{T}_h^i}\eta_{T,2}^2 + \sum_{e\in\mathcal{T}_h^\gamma}\eta_{e,\gamma,2}^2\right)^{\frac{1}{2}}. \qquad (3.1)
$$

Proof For any $r^* \in Q$, we let $\overline{q}^* \in Q'$ be the function defined by

$$L(\overline{q}^*, r^*) = b(\boldsymbol{u}^* - \boldsymbol{u}_h^*, r^*) = \sum_{i=1}^{2}(q_i - \nabla \cdot \boldsymbol{u}_h^i, r_i)_{\Omega_i} + (\widehat{q}_\gamma - \nabla_{\boldsymbol{\tau}} \cdot \widehat{\boldsymbol{u}}_h^\gamma + [\![\boldsymbol{u}_h \cdot \boldsymbol{n}]\!]_\gamma, \widehat{r}_\gamma)_\gamma.$$

Let $(\overline{\boldsymbol{u}}^*, \overline{p}^*)$ be the solution of the following variational formulation:

$$\begin{aligned} a(\overline{\boldsymbol{u}}^*, \boldsymbol{v}^*) - b(\boldsymbol{v}^*, \overline{p}^*) &= 0 \quad \forall\, \boldsymbol{v}^* \in \boldsymbol{U}^0, \\ b(\overline{\boldsymbol{u}}^*, r^*) &= L(\overline{q}^*, r^*) \quad \forall\, r^* \in Q. \end{aligned}$$

Clearly, we have

$$\begin{aligned} \|\overline{\boldsymbol{u}}^*\|_{\boldsymbol{U}} &\le C\|\overline{q}^*\|_{Q'} \\ &\le C\left(\sum_{i=1}^{2}\sum_{T\in\mathcal{T}_h^i}\|q_i - \nabla\cdot\boldsymbol{u}_h^i\|_{0,T}^2 + \sum_{e\in\mathcal{T}_h^\gamma}\|\widehat{q}_\gamma - \nabla_{\boldsymbol{\tau}}\cdot\widehat{\boldsymbol{u}}_h^\gamma + [\![\boldsymbol{u}_h\cdot\boldsymbol{n}]\!]_\gamma\|_{0,e}^2\right)^{\frac{1}{2}}. \end{aligned}$$

Due to the fact that $b(\boldsymbol{u}^* - \boldsymbol{u}_h^* - \overline{\boldsymbol{u}}^*, r^*) = 0$, we have $\boldsymbol{u}^* - \boldsymbol{u}_h^* - \overline{\boldsymbol{u}}^* \in \widetilde{\boldsymbol{U}}^0$. Furthermore, by the $\widetilde{\boldsymbol{U}}^0$-elliptic property of the bilinear form $a(\cdot,\cdot)$, we get

$$\begin{aligned} C\|\boldsymbol{u}^* - \boldsymbol{u}_h^* - \overline{\boldsymbol{u}}^*\|_{\boldsymbol{U}}^2 &\le a(\boldsymbol{u}^* - \boldsymbol{u}_h^* - \overline{\boldsymbol{u}}^*, \boldsymbol{u}^* - \boldsymbol{u}_h^* - \overline{\boldsymbol{u}}^*) \\ &\le a(\boldsymbol{u}^* - \boldsymbol{u}_h^*, \boldsymbol{u}^* - \boldsymbol{u}_h^* - \overline{\boldsymbol{u}}) + C\|\overline{\boldsymbol{u}}^*\|_{\boldsymbol{U}^*}\|\boldsymbol{u}^* - \boldsymbol{u}_h^* - \overline{\boldsymbol{u}}^*\|_{\boldsymbol{U}}, \end{aligned}$$

which directly yields

$$C\|\boldsymbol{u}^* - \boldsymbol{u}_h^* - \overline{\boldsymbol{u}}^*\|_{\boldsymbol{U}} \le \sup_{\substack{\boldsymbol{v}^*\in\widetilde{\boldsymbol{U}}^0 \\ \boldsymbol{v}^*\neq 0}} \frac{a(\boldsymbol{u}^* - \boldsymbol{u}_h^*, \boldsymbol{v}^*)}{\|\boldsymbol{v}^*\|_{\boldsymbol{U}}} + \|\overline{\boldsymbol{u}}^*\|_{\boldsymbol{U}^*}.$$

Thus, combining the above estimate and the upper bound for $\|\overline{\boldsymbol{u}}^*\|_{\boldsymbol{U}}$, we obtain the desired estimate (3.1). □

In the sequel we will apply the Scott–Zhang interpolation operator $\mathcal{I}_h^i : H^1_{\Gamma_i^N}(\Omega_i) \to V_{\Gamma_i^N,h}$, where $H^1_{\Gamma_i^N}(\Omega_i) = \{\varphi \in H^1(\Omega_i) : \varphi|_{\Gamma_i^N} = 0\}$ and $V_{\Gamma_i^N,h} = \{v \in C^0(\Omega_i) : v|_{\Gamma_i^N} = 0,\ v|_T \in \mathbb{P}_{k+1}(T), \forall\, T \in \mathcal{T}_h^i\}$, $i = 1, 2$. One can define $\mathcal{I}_h^i$ via (cf. [35])

$$\mathcal{I}_h^i\varphi = \sum_{z\in\mathcal{N}_h(\Omega_i)}(\Pi_z\varphi)\psi_z.$$

where $\mathcal{N}_h(\Omega_i)$ is the set of degrees of freedom for $V_{\Gamma_i^N,h}$, ψ_z is the local basis function on z, $\Pi_z\varphi = \int_{\sigma_z}\varphi\theta_z$. Here σ_z is an adjustable edge or triangle, one can refer to [35] for the details. θ_z is the dual basis function of ψ_z on σ_z. Let $\mathcal{N}_h(\gamma)$ be the set of degrees

of freedom of $V_{\Gamma_i^N,h}$ restricted on $\mathcal{T}_h^\gamma$. Particularly, if $z \in \mathcal{N}_h(\gamma)\backslash\partial\gamma^N$, we choose $\sigma_z \in \mathcal{T}_h^\gamma$. The Scott–Zhang interpolation operator $\mathcal{I}_h^i$ has the following approximation properties (cf. [35,40]).

Lemma 3.2 *For any $T \in \mathcal{T}_h^i$ and $e \in \mathcal{E}_h^0(\Omega_i)\cup\mathcal{E}_h(\Gamma_i^D)\cup\mathcal{T}_h^\gamma$, $i = 1, 2$, the following estimates hold for any function $\varphi \in H^1(\Omega_i)$:*

$$\|\varphi - \mathcal{I}_h^i\varphi\|_{0,T} \le Ch_T|\varphi|_{1,\Omega_T},$$
$$\|\varphi - \mathcal{I}_h^i\varphi\|_{0,e} \le Ch_e^{\frac{1}{2}}|\varphi|_{1,\Omega_e},$$

where $\Omega_T = \cup\{T' \in \mathcal{T}_h^i : \overline{T'} \cap \overline{T} \ne \emptyset\}$ and $\Omega_e = \cup\{T' \in \mathcal{T}_h^i : \overline{T'} \cap \overline{e} \ne \emptyset\}$.

Lemma 3.3 *For any $e \in \mathcal{T}_h^\gamma$, the following estimates hold for any $\varphi \in H^1_{\Gamma_i^N}(\Omega_i)|_{i=1,2}$:*

$$\|\varphi - \mathcal{I}_h^i\varphi\|_{0,e} \le Ch_e\|\frac{d\varphi}{d\boldsymbol{s}}\|_{0,\omega_e}, \tag{3.2}$$
$$\left\|\frac{d\varphi}{d\boldsymbol{s}} - \frac{d\mathcal{I}_h^i\varphi}{d\boldsymbol{s}}\right\|_{0,e} \le C\|\frac{d\varphi}{d\boldsymbol{s}}\|_{0,\omega_e}, \tag{3.3}$$

where $\omega_e = \cup\{e' \in \mathcal{T}_h^\gamma : \overline{e'} \cap \overline{e} \ne \emptyset\}$.

Based on Lemma 3.1, we continue to estimate the upper bound for $\|\boldsymbol{u}^* - \boldsymbol{u}_h^*\|_{\boldsymbol{U}}$. For any $\boldsymbol{v}^* \in \widetilde{\boldsymbol{U}}^0$, we observe from the Eqs. (2.3) and (2.4) that for any $\boldsymbol{v}_h^* \in \boldsymbol{U}_h^0$ there holds

$$\begin{aligned} a(\boldsymbol{u}^* - \boldsymbol{u}_h^*, \boldsymbol{v}^*) &= a(\boldsymbol{u}^*, \boldsymbol{v}^*) - a(\boldsymbol{u}_h^*, \boldsymbol{v}^* - \boldsymbol{v}_h^*) - a(\boldsymbol{u}_h^*, \boldsymbol{v}_h^*) \\ &= b(\boldsymbol{v}^*, p^*) + G(g^D, \boldsymbol{v}^*) - a(\boldsymbol{u}_h^*, \boldsymbol{v}^* - \boldsymbol{v}_h^*) - b(\boldsymbol{v}_h^*, p_h^*) - G(g^D, \boldsymbol{v}_h^*) \\ &= -E(\boldsymbol{v}^* - \boldsymbol{v}_h^*), \end{aligned} \tag{3.4}$$

where $E(\boldsymbol{v}^* - \boldsymbol{v}_h^*) = a(\boldsymbol{u}_h^*, \boldsymbol{v}^* - \boldsymbol{v}_h^*) - b(\boldsymbol{v}^* - \boldsymbol{v}_h^*, p_h^*) - G(g^D, \boldsymbol{v}^* - \boldsymbol{v}_h^*)$ and the above last equality holds due to the fact $\boldsymbol{v}^* \in \widetilde{\boldsymbol{U}}^0$.

Lemma 3.4 *For any $\boldsymbol{v}^* \in \widetilde{\boldsymbol{U}}^0$, there exists $\boldsymbol{v}_h^* \in \boldsymbol{U}_h^0$ such that*

$$E(\boldsymbol{v}^* - \boldsymbol{v}_h^*) \le C\left(\sum_{i=1}^{2}\left(\sum_{T\in\mathcal{T}_h^i}\eta_{T,1}^2 + \sum_{e\in\mathcal{E}_h^0(\Omega_i)}\eta_e^2 + \sum_{e\in\mathcal{E}_h(\Gamma_i^D)}\eta_{e,\Gamma_i^D}^2\right) + \sum_{e\in\mathcal{T}_h^\gamma}\left(\eta_{e,\gamma,1}^2 + \eta_{e,\gamma,3}^2\right) + \eta_{\partial\gamma^D}^2\right)^{\frac{1}{2}}\|\boldsymbol{v}^*\|_{\boldsymbol{U}}.$$

Proof The definition of $\widetilde{\boldsymbol{U}}^0$ yields that for any $\boldsymbol{v}^* = (\boldsymbol{v}_1, \boldsymbol{v}_2, \widehat{\boldsymbol{v}}_\gamma) \in \widetilde{\boldsymbol{U}}^0$, there hold

$$\nabla_{\boldsymbol{\tau}} \cdot \widehat{\boldsymbol{v}}_\gamma - [\![\boldsymbol{v} \cdot \boldsymbol{n}]\!]_\gamma = 0 \quad \text{and} \quad \nabla \cdot \boldsymbol{v}_i = 0, \quad \boldsymbol{v}_i \cdot \boldsymbol{n} \in L^2(\gamma), \quad i = 1, 2.$$

Since Ω_1 and Ω_2 are both simply connected, for $i = 1, 2$, there exists $\varphi_i \in H^1_{\Gamma_i^N}(\Omega_i)$ such that $\boldsymbol{v}_i = \mathbf{curl}\,\varphi_i$ (cf. [25]). Noting that $\mathbf{curl}\,\varphi_i \cdot \boldsymbol{n} = -\frac{d\varphi_i}{ds} \in L^2(\gamma)$, thus $\varphi_i|_\gamma \in H^1(\gamma)$. Then we get $\nabla_{\boldsymbol{\tau}} \cdot \widehat{\boldsymbol{v}}_\gamma = [\![\mathbf{curl}\,\varphi \cdot \boldsymbol{n}]\!]_\gamma$ which indicates $\frac{d(\widehat{\boldsymbol{v}}_\gamma \cdot \boldsymbol{\tau})}{ds} = -[\![\frac{d\varphi}{ds}]\!]_\gamma$. We see $\widehat{\boldsymbol{v}}_\gamma = -[\![\varphi]\!]_\gamma \boldsymbol{\tau} \in \boldsymbol{U}^0_\gamma$. Now we let $\boldsymbol{v}_h^i = \mathbf{curl}\,\mathcal{I}_h^i \varphi_i \in \boldsymbol{U}^0_{i,h}$ for $i = 1, 2$ and $\widehat{\boldsymbol{v}}_h^\gamma = -[\![\mathcal{I}_h \varphi]\!]_\gamma \boldsymbol{\tau} \in \boldsymbol{U}^0_{\gamma,h}$. In the following, for any function F, we denote $[\![F(\mathcal{I}_h\varphi)]\!]_\gamma = F(\mathcal{I}_h^1\varphi_1)|_\gamma - F(\mathcal{I}_h^2\varphi_2)|_\gamma$ and $\{F(\mathcal{I}_h\varphi)\}_\gamma = \frac{1}{2}(F(\mathcal{I}_h^1\varphi_1)|_\gamma + F(\mathcal{I}_h^2\varphi_2)|_\gamma)$. Clearly, we have $[\![\boldsymbol{v}_h \cdot \boldsymbol{n}]\!]_\gamma = [\![\mathbf{curl}\,\mathcal{I}_h\varphi \cdot \boldsymbol{n}]\!]_\gamma = -[\![\frac{d\mathcal{I}_h\varphi}{ds}]\!]_\gamma = \nabla_{\boldsymbol{\tau}} \cdot \widehat{\boldsymbol{v}}_h^\gamma$. Therefore, there hold $b(\boldsymbol{v}^* - \boldsymbol{v}_h^*, p_h^*) = 0$ and $E(\boldsymbol{v}^* - \boldsymbol{v}_h^*) = a(\boldsymbol{u}_h^*, \boldsymbol{v}^* - \boldsymbol{v}_h^*) - G(g^D, \boldsymbol{v}^* - \boldsymbol{v}_h^*)$. According to the definition of the bilinear form $a(\cdot, \cdot)$, we get

$$\begin{aligned} a(\boldsymbol{u}_h^*, \boldsymbol{v}^* - \boldsymbol{v}_h^*) = \sum_{i=1}^2 &(\boldsymbol{K}_i^{-1}\boldsymbol{u}_h^i, \mathbf{curl}\,\varphi_i - \mathbf{curl}\,\mathcal{I}_h^i\varphi_i)_{\Omega_i} + (\widehat{\eta}_\gamma \widehat{\boldsymbol{u}}_h^\gamma, (-[\![\varphi]\!]_\gamma + [\![\mathcal{I}_h\varphi]\!]_\gamma)\boldsymbol{\tau})_\gamma \\ &+ (\eta_\gamma\{\boldsymbol{u}_h \cdot \boldsymbol{n}\}_\gamma, \{(\mathbf{curl}\,\varphi - \mathbf{curl}\,\mathcal{I}_h\varphi) \cdot \boldsymbol{n}\}_\gamma)_\gamma \\ &+ (\xi_\gamma \eta_\gamma [\![\boldsymbol{u}_h \cdot \boldsymbol{n}]\!]_\gamma, [\![(\mathbf{curl}\,\varphi - \mathbf{curl}\,\mathcal{I}_h\varphi) \cdot \boldsymbol{n}]\!]_\gamma)_\gamma. \end{aligned}$$

By integration by parts, we deduce that $E(\boldsymbol{v}^* - \boldsymbol{v}_h^*) = T_1 + T_2 + T_3 + T_4 + T_5$, where

$$\begin{aligned} T_1 &= \sum_{i=1}^2 \sum_{T \in \mathcal{T}_h^i} \big(\mathrm{curl}\,(\boldsymbol{K}_i^{-1}\boldsymbol{u}_h^i), \varphi_i - \mathcal{I}_h^i\varphi_i\big)_T + \sum_{i=1}^2 \sum_{e \in \mathcal{E}_h^0(\Omega_i)} \big([\![\boldsymbol{K}_i^{-1}\boldsymbol{u}_h^i \cdot \boldsymbol{s}]\!], \varphi_i - \mathcal{I}_h^i\varphi_i\big)_e, \\ T_2 &= \sum_{i=1}^2 \sum_{e \in \mathcal{E}_h(\Gamma_i^D)} \left(\boldsymbol{K}_i^{-1}\boldsymbol{u}_h^i \cdot \boldsymbol{s} + \frac{dg_i^D}{ds}, \varphi_i - \mathcal{I}_h^i\varphi_i\right)_e, \\ T_3 &= \sum_{e \in \mathcal{T}_h^\gamma} \int_e [\![(\boldsymbol{K}^{-1}\boldsymbol{u}_h \cdot \boldsymbol{\tau})(\varphi - \mathcal{I}_h\varphi)]\!]_\gamma - \left(\eta_\gamma\{\boldsymbol{u}_h \cdot \boldsymbol{n}\}_\gamma, \left\{\frac{d\varphi}{ds} - \frac{d\mathcal{I}_h\varphi}{ds}\right\}_\gamma\right)_\gamma, \\ T_4 &= -(\widehat{\eta}_\gamma \widehat{\boldsymbol{u}}_h^\gamma \cdot \boldsymbol{\tau}, [\![\varphi - \mathcal{I}_h\varphi]\!]_\gamma)_\gamma - \left(\xi_\gamma\eta_\gamma [\![\boldsymbol{u}_h \cdot \boldsymbol{n}]\!]_\gamma, \left[\!\!\left[\frac{d\varphi}{ds} - \frac{d\mathcal{I}_h\varphi}{ds}\right]\!\!\right]_\gamma\right)_\gamma, \\ T_5 &= -(\widehat{g}_\gamma^D, [\![\varphi - \mathcal{I}_h\varphi]\!]_\gamma)_{\partial\gamma^D} + [\![g^D(\varphi - \mathcal{I}_h\varphi)]\!]_{\partial\gamma^D}. \end{aligned}$$

Here, for any function ψ_i defined in Ω_i, we let $[\![\psi]\!]_{\partial\gamma^D} = \psi_1|_{\partial\gamma^D} - \psi_2|_{\partial\gamma^D}$. Applying the local approximation property of $\mathcal{I}_h^i|_{i=1,2}$ in Lemma 3.2, we obtain

$$\begin{aligned} CT_1 \le &\sum_{i=1}^2 \sum_{T \in \mathcal{T}_h^i} h_T \|\mathrm{curl}\,(\boldsymbol{K}_i^{-1}\boldsymbol{u}_h^i)\|_{0,T} |\varphi_i|_{1,\Omega_T} \\ &+ \sum_{i=1}^2 \sum_{e \in \mathcal{E}_h^0(\Omega_i)} h_e^{\frac{1}{2}} \|[\![\boldsymbol{K}_i^{-1}\boldsymbol{u}_h^i \cdot \boldsymbol{s}]\!]\|_{0,e} |\varphi_i|_{1,\Omega_e}, \end{aligned}$$

$$CT_2 \leq \sum_{i=1}^{2} \sum_{e\in\mathcal{E}_h(\Gamma_i^D)} h_e^{\frac{1}{2}} \|\boldsymbol{K}_i^{-1}\boldsymbol{u}_h^i\cdot\boldsymbol{s} + \frac{dg_i^D}{d\boldsymbol{s}}\|_{0,e}|\varphi_i|_{1,\Omega_e}.$$

We now employ the interpolation operators $\Pi_h^i|_{i=1,2}$ and Π_h^γ defined in (2.5) and (2.6) to deduce the upper bounds for T_3 and T_4. For any function F, we denote $[\![F(\Pi_h p_h)]\!]_\gamma = F(\Pi_h^1 p_h^1)|_\gamma - F(\Pi_h^2 p_h^2)|_\gamma$ and $\{F(\Pi_h p_h)\}_\gamma = \frac{1}{2}(F(\Pi_h^1 p_h^1)|_\gamma + F(\Pi_h^2 p_h^2)|_\gamma)$. T_3 can be written as

$$\begin{aligned}
T_3 &= \sum_{e\in\mathcal{T}_h^\gamma}\int_e [\![(\boldsymbol{K}^{-1}\boldsymbol{u}_h\cdot\boldsymbol{\tau} + \nabla\Pi_h p_h\cdot\boldsymbol{\tau})(\varphi-\mathcal{I}_h\varphi)]\!]_\gamma + \left(\{\Pi_h p_h\}_\gamma, \left[\!\!\left[\frac{d\varphi}{d\boldsymbol{s}} - \frac{d\mathcal{I}_h\varphi}{d\boldsymbol{s}}\right]\!\!\right]_\gamma\right)_\gamma \\
&\quad + \left([\![\Pi_h p_h]\!]_\gamma - \eta_\gamma\{\boldsymbol{u}_h\cdot\boldsymbol{n}\}_\gamma, \left\{\frac{d\varphi}{d\boldsymbol{s}} - \frac{d\mathcal{I}_h\varphi}{d\boldsymbol{s}}\right\}_\gamma\right)_\gamma - [\![\Pi_h p_h(\varphi-\mathcal{I}_h\varphi)]\!]_{\partial\gamma^D} \\
&= \sum_{e\in\mathcal{T}_h^\gamma}\int_e [\![(\boldsymbol{K}^{-1}\boldsymbol{u}_h\cdot\boldsymbol{\tau} + \nabla p_h\cdot\boldsymbol{\tau})(\varphi-\mathcal{I}_h\varphi)]\!]_\gamma + \left(\{p_h\}_\gamma, \left[\!\!\left[\frac{d\varphi}{d\boldsymbol{s}} - \frac{d\mathcal{I}_h\varphi}{d\boldsymbol{s}}\right]\!\!\right]_\gamma\right)_\gamma \\
&\quad + \sum_{e\in\mathcal{T}_h^\gamma}\int_e [\![(\nabla\Pi_h p_h\cdot\boldsymbol{\tau} - \nabla p_h\cdot\boldsymbol{\tau})(\varphi-\mathcal{I}_h\varphi)]\!]_\gamma \\
&\quad + \sum_{e\in\mathcal{T}_h^\gamma}\int_e \left[\!\!\left[(\Pi_h p_h - p_h)\left(\frac{d\varphi}{d\boldsymbol{s}} - \frac{d\mathcal{I}_h\varphi}{d\boldsymbol{s}}\right)\right]\!\!\right]_\gamma \\
&\quad + \left([\![p_h]\!]_\gamma - \eta_\gamma\{\boldsymbol{u}_h\cdot\boldsymbol{n}\}_\gamma, \left\{\frac{d\varphi}{d\boldsymbol{s}} - \frac{d\mathcal{I}_h\varphi}{d\boldsymbol{s}}\right\}_\gamma\right)_\gamma - [\![p_h(\varphi-\mathcal{I}_h\varphi)]\!]_{\partial\gamma^D}.
\end{aligned}$$

For T_4, we have

$$\begin{aligned}
T_4 &= -(\widehat{z\eta}_\gamma\widehat{\boldsymbol{u}}_h^\gamma\cdot\boldsymbol{\tau} + \nabla_{\boldsymbol{\tau}}\Pi_h^\gamma\widehat{p}_h^\gamma\cdot\boldsymbol{\tau}, [\![\varphi-\mathcal{I}_h\varphi]\!]_\gamma)_\gamma - \left(\Pi_h^\gamma\widehat{p}_h^\gamma, \left[\!\!\left[\frac{d\varphi}{d\boldsymbol{s}} - \frac{d\mathcal{I}_h\varphi}{d\boldsymbol{s}}\right]\!\!\right]_\gamma\right)_\gamma \\
&\quad - \left(\xi_\gamma\eta_\gamma[\![\boldsymbol{u}_h\cdot\boldsymbol{n}]\!]_\gamma, \left[\!\!\left[\frac{d\varphi}{d\boldsymbol{s}} - \frac{d\mathcal{I}_h\varphi}{d\boldsymbol{s}}\right]\!\!\right]_\gamma\right)_\gamma + (\Pi_h^\gamma\widehat{p}_h^\gamma, [\![\varphi-\mathcal{I}_h\varphi]\!]_\gamma)_{\partial\gamma^D} \\
&= -(\widehat{\eta}_\gamma\widehat{\boldsymbol{u}}_h^\gamma\cdot\boldsymbol{\tau} + \nabla_{\boldsymbol{\tau}}\widehat{p}_h^\gamma\cdot\boldsymbol{\tau}, [\![\varphi-\mathcal{I}_h\varphi]\!]_\gamma)_\gamma - \left(\widehat{p}_h^\gamma + \xi_\gamma\eta_\gamma[\![\boldsymbol{u}_h\cdot\boldsymbol{n}]\!]_\gamma, \left[\!\!\left[\frac{d\varphi}{d\boldsymbol{s}} - \frac{d\mathcal{I}_h\varphi}{d\boldsymbol{s}}\right]\!\!\right]_\gamma\right)_\gamma \\
&\quad + (\nabla_{\boldsymbol{\tau}}\widehat{p}_h^\gamma\cdot\boldsymbol{\tau} - \nabla_{\boldsymbol{\tau}}\Pi_h^\gamma\widehat{p}_h^\gamma\cdot\boldsymbol{\tau}, [\![\varphi-\mathcal{I}_h\varphi]\!]_\gamma)_\gamma \\
&\quad + \left(\widehat{p}_h^\gamma - \Pi_h^\gamma\widehat{p}_h^\gamma, \left[\!\!\left[\frac{d\varphi}{d\boldsymbol{s}} - \frac{d\mathcal{I}_h\varphi}{d\boldsymbol{s}}\right]\!\!\right]_\gamma\right)_\gamma + (\widehat{p}_h^\gamma, [\![\varphi-\mathcal{I}_h\varphi]\!]_\gamma)_{\partial\gamma^D}.
\end{aligned}$$

By the definition of the Scott–Zhang interpolation operator and shape regularity of the mesh, we can deduce that

$$\left|(\varphi_i - \mathcal{I}_h^i\varphi_i)|_{\partial\gamma^D}\right| \leq Ch_{e_d}^{\frac{1}{2}}\left\|\frac{d\varphi_i}{d\boldsymbol{s}}\right\|_{\omega_{e_d}}, \quad i=1,2. \tag{3.5}$$

Then, combining the above equalities for T_3 and T_4, the inverse inequality, (3.5) and the local approximation property of $\mathcal{I}_h^i|_{i=1,2}$ in Lemma 3.3, we deduce that

$$\begin{aligned} C(T_3+T_4+T_5) \le \sum_{i=1}^{2}\sum_{e\in\mathcal{T}_h^\gamma} \big(& h_e\|\boldsymbol{K}_i^{-1}\boldsymbol{u}_h^i\cdot\boldsymbol{\tau}+\nabla p_h^i\cdot\boldsymbol{\tau}\|_{0,e}+\|[\![p_h]\!]_\gamma-\eta_\gamma\{\boldsymbol{u}_h\cdot\boldsymbol{n}\}_\gamma\|_{0,e} \\ & + h_e\|\widehat{\eta}_\gamma\widehat{\boldsymbol{u}}_h^\gamma\cdot\boldsymbol{\tau}+\nabla_{\boldsymbol{\tau}}\widehat{p}_h^\gamma\cdot\boldsymbol{\tau}\|_{0,e}+\|\{p_h\}_\gamma-\widehat{p}_h^\gamma-\xi_\gamma\eta_\gamma[\![\boldsymbol{u}_h\cdot\boldsymbol{n}]\!]_\gamma\|_{0,e} \\ & + \|p_h^i-\Pi_h^i p_h^i\|_{0,e}+\|\widehat{p}_h^\gamma-\Pi_h^\gamma\widehat{p}_h^\gamma\|_{0,e}\big)\left\|\frac{d\varphi_i}{d\boldsymbol{s}}\right\|_{0,\omega_e} \\ & + \left(\sum_{i=1}^{2} h_{e_d}^{\frac{1}{2}}|g_i^D-(p_h^i|_{T_i^*})|_{\partial\gamma^D}|+h_{e_d}^{\frac{1}{2}}|\widehat{g}_\gamma^D-\widehat{p}_h^\gamma|_{\partial\gamma^D}|\right)\left\|\frac{d\varphi_i}{d\boldsymbol{s}}\right\|_{\omega_{e_d}}. \end{aligned}$$

Noting that $\|\mathbf{curl}\,\varphi_i\|_{0,\Omega_i}^2=|\varphi_i|_{1,\Omega_i}^2$, we observe that

$$\sum_{i=1}^{2}\left(|\varphi_i|_{1,\Omega_i}^2+\left\|\frac{d\varphi_i}{d\boldsymbol{s}}\right\|_{0,\gamma}^2\right)\le\|\boldsymbol{v}^*\|_U^2.$$

Then, we obtain the desired result by the estimates of the upper bounds for T_1, T_2, T_3, T_4, T_5 and the Cauchy–Schwarz inequality.

Now we can conclude the a posteriori error estimate for $\|\boldsymbol{u}^*-\boldsymbol{u}_h^*\|_U$.

Lemma 3.5 *There exists a positive constant C such that*

$$\begin{aligned} C\|\boldsymbol{u}^*-\boldsymbol{u}_h^*\|_U \le \Bigg(\sum_{i=1}^{2}\Bigg(\sum_{T\in\mathcal{T}_h^i}(\eta_{T,1}^2+\eta_{T,2}^2)+\sum_{e\in\mathcal{E}_h^0(\Omega_i)}\eta_e^2+\sum_{e\in\mathcal{E}_h(\Gamma_i^D)}\eta_{e,\Gamma_i^D}^2\Bigg) \\ +\sum_{e\in\mathcal{T}_h^\gamma}\eta_{e,\gamma}^2+\eta_{\partial\gamma^D}^2\Bigg)^{\frac{1}{2}}. \end{aligned}$$

Proof The desired estimate is a straightforward result of Lemma 3.1, the equality (3.4) and Lemma 3.4.

We are now in a position to provide the upper bound for $\|p^*-p_h^*\|_Q$. In the proof of the full continuous *inf–sup* condition (cf. the second part of proof in Theorem 4.1 in [31]), a partial continuous *inf–sup* condition holds as

$$C\|p^*-p_h^*\|_Q\le\sup_{\substack{\boldsymbol{v}^*\in\boldsymbol{U}^0\\ \boldsymbol{v}^*\neq0,[\![\boldsymbol{v}\cdot\boldsymbol{n}]\!]_\gamma=0}}\frac{b(\boldsymbol{v}^*,p^*-p_h^*)}{\|\boldsymbol{v}^*\|_U}. \tag{3.6}$$

For any nonzero $\boldsymbol{v}^* = (\boldsymbol{v}_1, \boldsymbol{v}_2, \widehat{\boldsymbol{v}}_\gamma) \in \boldsymbol{U}^0$ with $[\![\boldsymbol{v}\cdot\boldsymbol{n}]\!]_\gamma = 0$, we assume $\widetilde{\boldsymbol{v}} \in H_{\Gamma^N}(\mathrm{div},\Omega)$ satisfying $\widetilde{\boldsymbol{v}}|_{\Omega_1} = \boldsymbol{v}_1$ and $\widetilde{\boldsymbol{v}}|_{\Omega_2} = \boldsymbol{v}_2$, where $H_{\Gamma^N}(\mathrm{div},\Omega) = \{\boldsymbol{v} \in H(\mathrm{div},\Omega) : \ \boldsymbol{v}\cdot\boldsymbol{n}_{\Gamma^N} = 0, \Gamma^N \subset \partial\Omega\}$. By the Helmholtz decomposition of the space $H_{\Gamma^N}(\mathrm{div},\Omega)$ (cf. [26]), there exist $\widetilde{\varphi} \in H^1_{\Gamma^N}(\Omega)$ and $\widetilde{\boldsymbol{w}} \in [H^1_{\Gamma^N}(\Omega)]^2$ such that $\widetilde{\boldsymbol{v}} = \mathbf{curl}\,\widetilde{\varphi} + \widetilde{\boldsymbol{w}}$ and the stability estimate $\|\widetilde{\varphi}\|_{1,\Omega} + \|\widetilde{\boldsymbol{w}}\|_{1,\Omega} \le C\|\nabla\cdot\widetilde{\boldsymbol{v}}\|_{0,\Omega}$ holds true, where $H^1_{\Gamma^N}(\Omega) = \{\psi \in H^1(\Omega) : \ \psi = 0 \text{ on } \Gamma^N,\ \Gamma^N \subset \partial\Omega\}$. We let $\boldsymbol{w}_i = \widetilde{\boldsymbol{w}}|_{\Omega_i}, i = 1,2$, then $\boldsymbol{w}_i \in [H^1(\Omega_i)]^2 \cap \boldsymbol{U}_i^0$ and there hold $\nabla\cdot\boldsymbol{v}_i = \nabla\cdot\boldsymbol{w}_i$, $[\![\boldsymbol{w}\cdot\boldsymbol{n}]\!]_\gamma = 0$ and

$$\sum_{i=1}^{2}\|\boldsymbol{w}_i\|_{1,\Omega_i} \le C\|\nabla\cdot\widetilde{\boldsymbol{v}}\|_{0,\Omega} = C\sum_{i=1}^{2}\|\nabla\cdot\boldsymbol{v}_i\|_{0,\Omega_i}. \tag{3.7}$$

On the reduced fracture γ, there also exists $\widehat{\boldsymbol{w}}_\gamma \in [H^1(\gamma)]^2 \cap \boldsymbol{U}_\gamma^0$ such that $\nabla_{\boldsymbol{\tau}}\cdot\widehat{\boldsymbol{w}}_\gamma = \nabla_{\boldsymbol{\tau}}\cdot\widehat{\boldsymbol{v}}_\gamma$, and there holds

$$\|\widehat{\boldsymbol{w}}_\gamma\|_{1,\gamma} \le C\|\nabla_{\boldsymbol{\tau}}\cdot\widehat{\boldsymbol{v}}_\gamma\|_{0,\gamma}. \tag{3.8}$$

Indeed, this can be immediately obtained by the similar auxiliary problem stated in the proof of Theorem 4.1 in [31]. Let $\boldsymbol{w}^* = (\boldsymbol{w}_1, \boldsymbol{w}_2, \widehat{\boldsymbol{w}}_\gamma)$. Now we further observe from the Eqs. (2.3) and (2.4) that, for any $\boldsymbol{w}_h^* \in \boldsymbol{U}_h^0$, there holds

$$\begin{aligned}
b(\boldsymbol{v}^*, p^* - p_h^*) &= b(\boldsymbol{w}^*, p^* - p_h^*)\\
&= a(\boldsymbol{u}^*, \boldsymbol{w}^*) - a(\boldsymbol{u}_h^*, \boldsymbol{w}^*) + a(\boldsymbol{u}_h^*, \boldsymbol{w}^*) - b(\boldsymbol{w}^*, p_h^*) - G(g^D, \boldsymbol{w}^*)\\
&= a(\boldsymbol{u}^* - \boldsymbol{u}_h^*, \boldsymbol{w}^*) + a(\boldsymbol{u}_h^*, \boldsymbol{w}^*) - b(\boldsymbol{w}_h^*, p_h^*) - b(\boldsymbol{w}^* - \boldsymbol{w}_h^*, p_h^*) - G(g^D, \boldsymbol{w}^*)\\
&= a(\boldsymbol{u}^* - \boldsymbol{u}_h^*, \boldsymbol{w}^*) + a(\boldsymbol{u}_h^*, \boldsymbol{w}^* - \boldsymbol{w}_h^*) - b(\boldsymbol{w}^* - \boldsymbol{w}_h^*, p_h^*) - G(g^D, \boldsymbol{w}^* - \boldsymbol{w}_h^*).
\end{aligned} \tag{3.9}$$

Using (3.7) and (3.8), it is clear that

$$a(\boldsymbol{u}^* - \boldsymbol{u}_h^*, \boldsymbol{w}^*) \le C\|\boldsymbol{u}^* - \boldsymbol{u}_h^*\|_U\|\boldsymbol{v}^*\|_U. \tag{3.10}$$

The upper bound for $\|\boldsymbol{u}^* - \boldsymbol{u}_h^*\|_U$ has been obtained. Next, we will utilize $H(\mathrm{div})$-conforming interpolation operator to get the upper bound for the remaining terms

$$R(\boldsymbol{w}^* - \boldsymbol{w}_h^*) = a(\boldsymbol{u}_h^*, \boldsymbol{w}^* - \boldsymbol{w}_h^*) - b(\boldsymbol{w}^* - \boldsymbol{w}_h^*, p_h^*) - G(g^D, \boldsymbol{w}^* - \boldsymbol{w}_h^*).$$

For $i = 1,2$, there exists $H(\mathrm{div})$-conforming interpolation operator

$$\boldsymbol{\Pi}_{i,h}^{\mathrm{div}} : [H^1(\Omega_i)]^2_{\Gamma_i^N} \to \boldsymbol{U}_{i,h}^0$$

such that (cf., e.g., [11,15,18])

$$\nabla\cdot(\boldsymbol{\Pi}_{i,h}^{\mathrm{div}}\boldsymbol{\psi}) = \mathcal{P}_T(\nabla\cdot\boldsymbol{\psi}) \quad \forall\,\boldsymbol{\psi} \in [H^1(\Omega_i)]^2_{\Gamma_i^N},\ \forall\, T \in \mathcal{T}_h^i, \tag{3.11}$$

$$(\boldsymbol{\Pi}_{i,h}^{\mathrm{div}}\boldsymbol{\psi})\cdot\boldsymbol{n}_e = \mathcal{P}_e(\boldsymbol{\psi}\cdot\boldsymbol{n}_e)\quad \forall\,\boldsymbol{\psi}\in[H^1(\Omega_i)]^2_{\Gamma_i^N},\ \forall\, e\in\mathcal{E}_h(\Omega_i), \tag{3.12}$$

where $[H^1(\Omega_i)]^2_{\Gamma_i^N} = \{\boldsymbol{\psi}\in[H^1(\Omega_i)]^2 :\ \boldsymbol{\psi}\cdot\boldsymbol{n}_{\Gamma_i^N} = 0 \text{ on } \Gamma_i^N\}$. Moreover, the $H(\mathrm{div})$-conforming interpolation operator satisfies local error estimates

$$\|\boldsymbol{\psi}-\boldsymbol{\Pi}_{i,h}^{\mathrm{div}}\boldsymbol{\psi}\|_{0,T}\le Ch_T\|\boldsymbol{\psi}\|_{1,T}\quad \forall\, T\in\mathcal{T}_h^i, \forall\,\boldsymbol{\psi}\in[H^1(\Omega_i)]^2_{\Gamma_i^N}, i=1,2, \tag{3.13}$$

$$\|\boldsymbol{\psi}-\boldsymbol{\Pi}_{i,h}^{\mathrm{div}}\boldsymbol{\psi}\|_{0,e}\le Ch_e^{\frac{1}{2}}\|\boldsymbol{\psi}\|_{1,T_e}\quad \forall\, e\in\mathcal{E}_h(\Omega_i), \forall\,\boldsymbol{\psi}\in[H^1(\Omega_i)]^2_{\Gamma_i^N}, i=1,2, \tag{3.14}$$

where T_e is an element in $\mathcal{T}_h^i$ such that $e\subset\partial T_e$.

On the reduced fracture γ, we can apply the standard continuous piecewise interpolation operator or the projection-based interpolation operator (cf. [18]) $I_h^\gamma : H^1_{\partial\gamma^N}(\gamma)\to H^1_{\partial\gamma^N}(\gamma)\cap(\boldsymbol{U}^0_{\gamma,h}\cdot\boldsymbol{\tau})$ which satisfies

$$\sum_{e\in\mathcal{T}_h^\gamma} h_e^{-2}\|\psi-I_h^\gamma\psi\|^2_{0,e}\le C\left\|\frac{d\psi}{d\boldsymbol{s}}\right\|^2_\gamma, \tag{3.15}$$

where $H^1_{\partial\gamma^N}(\gamma)=\{\psi\in H^1(\gamma):\ \psi=0 \text{ at } \partial\gamma^N\}$.

Lemma 3.6 *Let $\boldsymbol{w}^*$ be defined above and $\boldsymbol{w}_h^* = (\boldsymbol{w}_h^1,\boldsymbol{w}_h^2,\widehat{\boldsymbol{w}}_h^\gamma)$ with $\boldsymbol{w}_h^i = \boldsymbol{\Pi}_{i,h}^{\mathrm{div}}\boldsymbol{w}_i$, $i=1,2$ and $\widehat{\boldsymbol{w}}_h^\gamma = I_h^\gamma(\widehat{\boldsymbol{w}}_\gamma\cdot\boldsymbol{\tau})\boldsymbol{\tau}$. Then there holds*

$$R(\boldsymbol{w}^*-\boldsymbol{w}_h^*)\le C\left(\sum_{i=1}^2\sum_{T\in\mathcal{T}_h^i}\eta^2_{T,3}+\sum_{e\in\mathcal{T}_h^\gamma}\eta^2_{e,\gamma,3}+\sum_{i=1}^2\sum_{e\in\mathcal{E}_h(\Gamma_i^D)}\mathrm{osc}^2_{e,1,\Gamma_i^D}\right)^{\frac{1}{2}}\|\boldsymbol{v}^*\|_{\boldsymbol{U}}.$$

Proof According to the definitions of the bilinear forms $a(\cdot,\cdot)$ and $b(\cdot,\cdot)$, we have

$$R(\boldsymbol{w}^*-\boldsymbol{w}_h^*) = S_1+S_2+S_3+S_4,$$

where

$$S_1=\sum_{i=1}^2\sum_{T\in\mathcal{T}_h^i}\Big((\boldsymbol{K}_i^{-1}\boldsymbol{u}_h^i,\boldsymbol{w}_i-\boldsymbol{w}_h^i)_T-(\nabla\cdot(\boldsymbol{w}_i-\boldsymbol{w}_h^i),p_h^i)_T\Big),$$

$$S_2=\sum_{e\in\mathcal{T}_h^e}\Big((\widehat{\eta}_\gamma\widehat{\boldsymbol{u}}_h^\gamma,\widehat{\boldsymbol{w}}_\gamma-\widehat{\boldsymbol{w}}_h^\gamma)_e-(\nabla_{\boldsymbol{\tau}}\cdot(\widehat{\boldsymbol{w}}_\gamma-\widehat{\boldsymbol{w}}_h^\gamma),\widehat{p}_h^\gamma)_e\Big),$$

$$S_3 = \sum_{e\in\mathcal{T}_h^\gamma} \Big(\big(\eta_\gamma \{\boldsymbol{u}_h\cdot\boldsymbol{n}\}_\gamma, \{(\boldsymbol{w}-\boldsymbol{w}_h)\cdot\boldsymbol{n}\}\big)_e + \big(\xi_\gamma\eta_\gamma [\![\boldsymbol{u}_h\cdot\boldsymbol{n}]\!]_\gamma, [\![(\boldsymbol{w}-\boldsymbol{w}_h)\cdot\boldsymbol{n}]\!]_\gamma\big)_e$$
$$+\big([\![(\boldsymbol{w}-\boldsymbol{w}_h)\cdot\boldsymbol{n}]\!]_\gamma, \widehat{p}_h^\gamma\big)_e\Big),$$
$$S_4 = -G(g^D, \boldsymbol{w}^* - \boldsymbol{w}_h^*).$$

By the properties (3.11)–(3.13) of $H(\mathrm{div})$-conforming interpolation operator, we deduce that

$$S_1 = \sum_{i=1}^{2}\sum_{T\in\mathcal{T}_h^i} \big(\boldsymbol{K}_i^{-1}\boldsymbol{u}_h^i + \nabla p_h^i, \boldsymbol{w}_i - \boldsymbol{w}_h^i\big)_T$$
$$\le C\sum_{i=1}^{2}\left(\sum_{T\in\mathcal{T}_h^i} h_T^2 \|\boldsymbol{K}_i^{-1}\boldsymbol{u}_h^i + \nabla p_h^i\|_{0,T}^2\right)^{\frac{1}{2}} \left(\sum_{i=1}^{2}\|\boldsymbol{w}_i\|_{1,\Omega_i}^2\right)^{\frac{1}{2}}.$$

By integration by parts and (3.15), we have

$$S_2 = \sum_{e\in\mathcal{T}_h^e} (\widehat{\eta}_\gamma\widehat{\boldsymbol{u}}_h^\gamma + \nabla_{\boldsymbol{\tau}}\widehat{p}_h^\gamma, \widehat{\boldsymbol{w}}_\gamma - \widehat{\boldsymbol{w}}_h^\gamma)_e$$
$$\le C\left(\sum_{e\in\mathcal{T}_h^e} h_e^2\|\widehat{\eta}_\gamma\widehat{\boldsymbol{u}}_h^\gamma + \nabla_{\boldsymbol{\tau}}\widehat{p}_h^\gamma\|_{0,e}^2\right)^{\frac{1}{2}} \left\|\frac{d(\widehat{\boldsymbol{w}}_\gamma\cdot\boldsymbol{\tau})}{d\boldsymbol{s}}\right\|_{0,\gamma}.$$

The property (3.12) and the fact that $\{\boldsymbol{u}_h\cdot\boldsymbol{n}\}_\gamma$, $[\![\boldsymbol{u}_h\cdot\boldsymbol{n}]\!]_\gamma$ and $\widehat{p}_h^\gamma$ are all piecewise linear on $\mathcal{T}_h^\gamma$ imply that $S_3 = 0$. Moreover, (3.12) and the property of I_h^γ imply that

$$S_4 = \sum_{i=1}^{2}\sum_{e\in\mathcal{E}_h(\Gamma_i^D)} \Big(g_i^D, (\boldsymbol{w}_i - \boldsymbol{w}_h^i)\cdot\boldsymbol{n}_\Gamma\Big)_e + (\widehat{g}_\gamma^D, (\widehat{\boldsymbol{w}}_\gamma - \widehat{\boldsymbol{w}}_h^\gamma)\cdot\boldsymbol{n}_\Gamma)_{\partial\gamma^D}$$
$$= \sum_{i=1}^{2}\sum_{e\in\mathcal{E}_h(\Gamma_i^D)} \Big(g_i^D, (\boldsymbol{w}_i - \boldsymbol{w}_h^i)\cdot\boldsymbol{n}_\Gamma\Big)_e$$
$$= \sum_{i=1}^{2}\sum_{e\in\mathcal{E}_h(\Gamma_i^D)} \Big(g_i^D - \mathcal{P}_e g_i^D, (\boldsymbol{w}_i - \boldsymbol{w}_h^i)\cdot\boldsymbol{n}_\Gamma\Big)_e$$
$$\le C\left(\sum_{i=1}^{2}\sum_{e\in\mathcal{E}_h(\Gamma_i^D)} \mathrm{osc}_{e,1,\Gamma_i^D}^2\right)^{\frac{1}{2}} \left(\sum_{i=1}^{2}\|\boldsymbol{w}_i\|_{1,\Omega_i}^2\right)^{\frac{1}{2}}.$$

The estimates for S_1, S_2, S_3 and S_4, together with (3.7) and (3.8), yield the desired result.

Next we can conclude the a posteriori error estimate for $\|p^* - p_h^*\|_Q$.

Lemma 3.7 *There exists a positive constant C such that*

$$\|p^* - p_h^*\|_Q \le C(\eta + \mathrm{osc}_{1,\Gamma^D}).$$

Proof The desired result directly follows from the partial continuous *inf–sup* condition (3.6), the identity (3.9), the estimate (3.10), the upper bound for $\|\boldsymbol{u}^* - \boldsymbol{u}_h^*\|_U$ in Lemma 3.5 and the estimate in Lemma 3.6.

Now we further consider the a posteriori error estimate for the error measured in the energy norm (2.7), which is the first desired estimate (2.8) in Theorem 2.1. Firstly, by the one-dimensional Newton–Cotes integration formula and the shape regularity of the mesh, it is easy to deduce that for any $r_h^* = (r_h^1, r_h^2, \widehat{r}_h^\gamma) \in Q_h$ and any $e \in \mathcal{T}_h^\gamma$, there holds

$$\begin{aligned}&\sum_{i=1}^{2} \sum_{z\in\partial e\cap\mathcal{N}_h^0(\gamma)} h_z[\![r_h^i]\!]_z^2 + \sum_{z\in\partial e\cap\mathcal{N}_h^0(\gamma)} h_z[\![\widehat{r}_h^\gamma]\!]_z^2 \\ &\quad\approx \sum_{i=1}^{2} \|r_h^i - \Pi_h^i r_h^i\|_{0,e}^2 + \|\widehat{r}_h^\gamma - \Pi_h^\gamma \widehat{r}_h^\gamma\|_{0,e}^2. \end{aligned} \tag{3.16}$$

Noting that when $(\boldsymbol{u}^*, p^*)$ is the solution of (2.3), it holds

$$\begin{aligned}|||(\boldsymbol{u}^* - \boldsymbol{u}_h^*, p^* - p_h^*)|||_h^2 &= \|\boldsymbol{u}^* - \boldsymbol{u}_h^*\|_U^2 + \|p^* - p_h^*\|_Q^2 \\ &+ \sum_{i=1}^{2} h_{e_d}\big(g_i^D - (p_h^i|_{T_i^*})|_{\partial\gamma^D}\big)^2 + h_{e_d}\big(\widehat{g}_\gamma^D - \widehat{p}_h^\gamma|_{\partial\gamma^D}\big)^2 \\ &+ \sum_{i=1}^{2} \sum_{z\in\mathcal{N}_h^0(\gamma)} h_z[\![p_h^i]\!]_z^2 + \sum_{z\in\mathcal{N}_h^0(\gamma)} h_z[\![\widehat{p}_h^\gamma]\!]_z^2 \\ &+ \sum_{e\in\mathcal{T}_h^\gamma} \Big(\|\{p_h\}_\gamma - \widehat{p}_h^\gamma - \xi_\gamma\eta_\gamma[\![\boldsymbol{u}_h\cdot\boldsymbol{n}]\!]_\gamma\|_{0,e}^2 + \|[\![p_h]\!]_\gamma - \eta_\gamma\{\boldsymbol{u}_h\cdot\boldsymbol{n}\}_\gamma\|_{0,e}^2\Big).\end{aligned}$$

Therefore, the estimate (2.8) in Theorem 2.1 immediately follows from (3.16), Lemmas 3.5 and 3.7.

4 Proof of efficiency estimate

In this section, we give the proof of local efficiency of the a posteriori error estimator, which addresses the estimate (2.9) in Theorem 2.1. In order to prove the local efficiency

of the a posteriori error estimator, proper element and face bubble functions will be useful. For any $T \in \mathcal{T}_h$, we denote by $B_T = \prod_{i=1}^{d+1} \lambda_i \in \mathbb{P}_3(T)$ the element bubble function in T, where λ_i is the linear nodal basis function at ith vertex in T. Actually, B_T satisfies $\mathrm{supp}(B_T) \subseteq T$, $B_T = 0$ on ∂T and $B_T \in [0, 1]$. For any $e \in \mathcal{E}_h$, there also exists proper face bubble function $B_e \in \mathbb{P}_2(e)$ such that $\mathrm{supp}(B_e) \subseteq \widetilde{\Omega}_e = \{T \in \mathcal{T}_h, e \subset \partial T\}$, $B_e = 0$ on $\partial T \backslash e$ for $T \in \widetilde{\Omega}_e$, and $B_e \in [0, 1]$. We will also utilize an extension operator $L : C(e) \to C(T)$ which satisfies $L(\varphi) \in \mathbb{P}_k(T)$ and $L(\varphi)|_e = \varphi$ for any $\varphi \in \mathbb{P}_k(e), e \subset \partial T$ (cf. [41]). The properties of bubble functions and the extension operator L are shown in the following lemma.

Lemma 4.1 (cf. [41,42]) *For any element $T \in \mathcal{T}_h$, a polynomial $\phi \in \mathbb{P}_k(T)$ and any edge $e \in \mathcal{E}_h$, a polynomial $\psi \in \mathbb{P}_k(e)$, the following estimates hold*:

$$
\begin{aligned}
&C_1 \|\phi\|_{0,T}^2 \le \|B_T^{\frac{1}{2}} \phi\|_{0,T}^2 \le C_2 \|\phi\|_{0,T}^2, \\
&C_3 \|\psi\|_{0,e}^2 \le \|B_e^{\frac{1}{2}} \psi\|_{0,e}^2 \le C_4 \|\psi\|_{0,e}^2, \\
&C_5 h_e \|\psi\|_{0,e}^2 \le \|B_e^{\frac{1}{2}} L(\psi)\|_{0,T}^2 \le C_6 h_e \|\psi\|_{0,e}^2.
\end{aligned}
$$

Now we start to verify the local efficiency of the a posteriori error estimator.

Lemma 4.2 *For each $T \in \mathcal{T}_h^i$, $i = 1, 2$, there hold*

$$
\eta_{T,1} \le C \|\boldsymbol{K}_i^{-1}(\boldsymbol{u}_i - \boldsymbol{u}_h^i)\|_{0,T}, \tag{4.1}
$$

$$
\eta_{T,2} = \|\nabla \cdot \boldsymbol{u}^i - \nabla \cdot \boldsymbol{u}_h^i\|_{0,T}, \tag{4.2}
$$

$$
\eta_{T,3} \le \big(h_T \|\boldsymbol{K}_i^{-1}(\boldsymbol{u}_i - \boldsymbol{u}_h^i)\|_{0,T} + \|p_i - p_h^i\|_{0,T}\big). \tag{4.3}
$$

Proof According to the Eq. (2.2b), we have

$$
\begin{aligned}
\|\mathrm{curl}\,(\boldsymbol{K}_i^{-1}\boldsymbol{u}_h^i)\|_{0,T}^2 &\le C \|B_T^{\frac{1}{2}} \mathrm{curl}\,(\boldsymbol{K}_i^{-1}\boldsymbol{u}_h^i)\|_{0,T}^2 \\
&= C\big(B_T \mathrm{curl}\,(\boldsymbol{K}_i^{-1}\boldsymbol{u}_h^i - \boldsymbol{K}_i^{-1}\boldsymbol{u}_i), \mathrm{curl}\,(\boldsymbol{K}_i^{-1}\boldsymbol{u}_h^i)\big)_T.
\end{aligned}
$$

By integration by parts and noting that $B_T = 0$ on ∂T, we get

$$
\begin{aligned}
\|\mathrm{curl}\,(\boldsymbol{K}_i^{-1}\boldsymbol{u}_h^i)\|_{0,T}^2 &\le C(\boldsymbol{K}_i^{-1}\boldsymbol{u}_h^i - \boldsymbol{K}_i^{-1}\boldsymbol{u}_i, \mathbf{curl}\,(B_T \mathrm{curl}\,(\boldsymbol{K}_i^{-1}\boldsymbol{u}_h^i)))_T \\
&\le C \|\boldsymbol{K}_i^{-1}(\boldsymbol{u}_i - \boldsymbol{u}_h^i)\|_{0,T} h_T^{-1} \|B_T \mathrm{curl}\,(\boldsymbol{K}_i^{-1}\boldsymbol{u}_h^i)\|_{0,T}.
\end{aligned}
$$

Then (4.1) follows from the definition of $\eta_{T,1}$ and the property of B_T mentioned in Lemma 4.1. The identity (4.2) directly follows the Eq. (2.2a). Again, by the Eq. (2.2b) and the property of the bubble function B_T, we get

$$
\begin{aligned}
&\|\boldsymbol{K}_i^{-1}\boldsymbol{u}_h^i + \nabla p_h^i\|_{0,T}^2 \\
&\quad \le C\big(B_T(\boldsymbol{K}_i^{-1}\boldsymbol{u}_h^i + \nabla p_h^i), \boldsymbol{K}_i^{-1}\boldsymbol{u}_h^i + \nabla p_h^i - \boldsymbol{K}_i^{-1}\boldsymbol{u}_i - \nabla p_i\big)_T \\
&\quad = C\big(B_T(\boldsymbol{K}_i^{-1}\boldsymbol{u}_h^i + \nabla p_h^i), \boldsymbol{K}_i^{-1}\boldsymbol{u}_h^i - \boldsymbol{K}_i^{-1}\boldsymbol{u}_i\big)_T \\
&\qquad + C\big(\nabla \cdot (B_T(\boldsymbol{K}_i^{-1}\boldsymbol{u}_h^i + \nabla p_h^i)), p_i - p_h^i\big)_T
\end{aligned}
$$

$$\leq C\|\boldsymbol{K}_i^{-1}\boldsymbol{u}_h^i + \nabla p_h^i\|_{0,T}\|\boldsymbol{K}_i^{-1}(\boldsymbol{u}_i - \boldsymbol{u}_h^i)\|_{0,T} + Ch_T^{-1}\|\boldsymbol{K}_i^{-1}\boldsymbol{u}_h^i + \nabla p_h^i\|_{0,T}\|p_i - p_h^i\|_{0,T}.$$

Then we obtain (4.3) by the above estimate.

Lemma 4.3 *For any $e \in \mathcal{E}_h^0(\Omega_i)$, $i = 1, 2$, there holds*

$$\eta_e \leq C \sum_{T \in \widetilde{\Omega}_e} \|\boldsymbol{K}_i^{-1}(\boldsymbol{u}_i - \boldsymbol{u}_h^i)\|_{0,T}.$$

Proof See Lemma 6.2 in [15].

Lemma 4.4 *For any $e \in \mathcal{E}_h(\Gamma_i^D)$, $i = 1, 2$, we have*

$$\eta_{e,\Gamma_i^D} \leq C\big(\|\boldsymbol{K}_i^{-1}(\boldsymbol{u}_i - \boldsymbol{u}_h^i)\|_{0,T_e} + \mathrm{osc}_{e,2,\Gamma_i^D}\big),$$

where T_e is an element in $\mathcal{T}_h^i$ such that $e \subset \partial T_e$.

Proof It is clear that

$$\eta_{e,\Gamma_i^D}^2 \leq h_e \left\| \boldsymbol{K}_i^{-1}\boldsymbol{u}_h^i \cdot \boldsymbol{s} + \frac{d\mathcal{P}_e g_i^D}{d\boldsymbol{s}} \right\|_{0,e}^2 + \mathrm{osc}_{e,2,\Gamma_i^D}^2. \tag{4.4}$$

By the property of bubble function B_e, we have

$$\left\| \boldsymbol{K}_i^{-1}\boldsymbol{u}_h^i \cdot \boldsymbol{s} + \frac{d\mathcal{P}_e g_i^D}{d\boldsymbol{s}} \right\|_{0,e}^2 \leq C \left(B_e \left(\boldsymbol{K}_i^{-1}\boldsymbol{u}_h^i \cdot \boldsymbol{s} + \frac{d\mathcal{P}_e g_i^D}{d\boldsymbol{s}} \right), \boldsymbol{K}_i^{-1}\boldsymbol{u}_h^i \cdot \boldsymbol{s} + \frac{dg_i^D}{d\boldsymbol{s}} + \frac{d\mathcal{P}_e g_i^D}{d\boldsymbol{s}} - \frac{dg_i^D}{d\boldsymbol{s}} \right)_e,$$

which, together with the Young's inequality, yields

$$\left\| \boldsymbol{K}_i^{-1}\boldsymbol{u}_h^i \cdot \boldsymbol{s} + \frac{d\mathcal{P}_e g_i^D}{d\boldsymbol{s}} \right\|_{0,e}^2 \leq C \left(G_1 + \left\| \frac{dg_i^D}{d\boldsymbol{s}} - \frac{d\mathcal{P}_e g_i^D}{d\boldsymbol{s}} \right\|_{0,e}^2 \right), \tag{4.5}$$

where $G_1 = \big(B_e(\boldsymbol{K}_i^{-1}\boldsymbol{u}_h^i \cdot \boldsymbol{s} + \frac{d\mathcal{P}_e g_i^D}{d\boldsymbol{s}}), \boldsymbol{K}_i^{-1}\boldsymbol{u}_h^i \cdot \boldsymbol{s} + \frac{dg_i^D}{d\boldsymbol{s}}\big)_e$. Since we assume $p_i|_e = g_i^D \in H^1(e)$, we can infer

$$G_1 = \left(B_e \left(\boldsymbol{K}_i^{-1} \boldsymbol{u}_h^i \cdot \boldsymbol{s} + \frac{d\mathcal{P}_e g_i^D}{d\boldsymbol{s}} \right), \boldsymbol{K}_i^{-1} \boldsymbol{u}_h^i \cdot \boldsymbol{s} + \nabla p_i \cdot \boldsymbol{s} \right)_e$$
$$= \left(B_e \left(\boldsymbol{K}_i^{-1} \boldsymbol{u}_h^i \cdot \boldsymbol{s} + \frac{d\mathcal{P}_e g_i^D}{d\boldsymbol{s}} \right), \boldsymbol{K}_i^{-1} (\boldsymbol{u}_h^i - \boldsymbol{u}_i) \cdot \boldsymbol{s} \right)_e .$$

By the property of the extension operator L and $B_e = 0$ on $\partial T_e \backslash e$, we deduce

$$G_1 = \left(\mathbf{curl} \left(B_e L \left(\boldsymbol{K}_i^{-1} \boldsymbol{u}_h^i \cdot \boldsymbol{s} + \frac{d\mathcal{P}_e g_i^D}{d\boldsymbol{s}} \right) \right), \boldsymbol{K}_i^{-1} (\boldsymbol{u}_h^i - \boldsymbol{u}_i) \right)_{T_e}$$
$$- \left(B_e L \left(\boldsymbol{K}_i^{-1} \boldsymbol{u}_h^i \cdot \boldsymbol{s} + \frac{d\mathcal{P}_e g_i^D}{d\boldsymbol{s}} \right), \operatorname{curl} (\boldsymbol{K}_i^{-1} \boldsymbol{u}_h^i) \right)_{T_e}$$
$$\leq C \left\| \boldsymbol{K}_i^{-1} \boldsymbol{u}_h^i \cdot \boldsymbol{s} + \frac{d\mathcal{P}_e g_i^D}{d\boldsymbol{s}} \right\|_{0,e}$$
$$\times \left(h_e^{-\frac{1}{2}} \| \boldsymbol{K}_i^{-1} (\boldsymbol{u}_i - \boldsymbol{u}_h^i) \|_{0,T_e} + C h_e^{\frac{1}{2}} \| \operatorname{curl} (\boldsymbol{K}_i^{-1} \boldsymbol{u}_h^i) \|_{0,T_e} \right),$$

which, together with (4.5) and (4.1), yields

$$h_e \left\| \boldsymbol{K}_i^{-1} \boldsymbol{u}_h^i \cdot \boldsymbol{s} + \frac{d\mathcal{P}_e g_i^D}{d\boldsymbol{s}} \right\|_{0,e}^2 \leq C \big(\| \boldsymbol{K}_i^{-1} (\boldsymbol{u}_i - \boldsymbol{u}_h^i) \|_{0,T_e}^2 + \operatorname{osc}_{e,2,\Gamma_i^D}^2 \big).$$

Hence, we conclude the desired result by the above estimate and (4.4).

Lemma 4.5 *For any $e \in \mathcal{T}_h^\gamma$, there holds*

$$C\eta_{e,\gamma,1}^2 \leq \sum_{i=1}^{2} \big(h_e \| \boldsymbol{K}_i^{-1} (\boldsymbol{u}_i - \boldsymbol{u}_h^i) \|_{0,T_e}^2 + \| (\boldsymbol{u}_i - \boldsymbol{u}_h^i) \cdot \boldsymbol{n} \|_{0,e}^2 \big) + \| \widehat{p}_\gamma - \widehat{p}_h^\gamma \|_{0,e}^2$$
$$+ \| \{p - p_h\}_\gamma - (\widehat{p}_\gamma - \widehat{p}_h^\gamma) - \xi_\gamma \eta_\gamma [\![(\boldsymbol{u} - \boldsymbol{u}_h) \cdot \boldsymbol{n}]\!]_\gamma \|_{0,e}^2$$
$$+ \| [\![p - p_h]\!]_\gamma - \eta_\gamma \{ (\boldsymbol{u} - \boldsymbol{u}_h) \cdot \boldsymbol{n} \}_\gamma \|_{0,e}^2$$
$$+ \sum_{i=1}^{2} \sum_{z \in \partial e \cap \mathcal{N}_h^0(\gamma)} h_z [\![p_i - p_h^i]\!]_z^2 + \sum_{z \in \partial e \cap \mathcal{N}_h^0(\gamma)} h_z [\![\widehat{p}_\gamma - \widehat{p}_h^\gamma]\!]_z^2.$$

Proof Since we assume that for any $e \in \mathcal{T}_h^\gamma$, $p_i|_e \in H^{\frac{1}{2}}(e), i = 1, 2$, then by the property of bubble function B_e, we have

$$C \| (\boldsymbol{K}_i^{-1} \boldsymbol{u}_h^i + \nabla p_h^i) \cdot \boldsymbol{\tau} \|_{0,e}^2$$
$$\leq \big(B_e (\boldsymbol{K}_i^{-1} \boldsymbol{u}_h^i + \nabla p_h^i) \cdot \boldsymbol{\tau}, (\boldsymbol{K}_i^{-1} \boldsymbol{u}_h^i + \nabla p_h^i) \cdot \boldsymbol{\tau} - (\boldsymbol{K}_i^{-1} \boldsymbol{u}_i + \nabla p_i) \cdot \boldsymbol{\tau} \big)_e.$$

Similar to the estimate of G_1 in Lemma 4.4, we can also deduce that

$$\begin{aligned}&\big(B_e(\boldsymbol{K}_i^{-1}\boldsymbol{u}_h^i+\nabla p_h^i)\cdot\boldsymbol{\tau},(\boldsymbol{K}_i^{-1}\boldsymbol{u}_h^i-\boldsymbol{K}_i^{-1}\boldsymbol{u}_i)\cdot\boldsymbol{\tau}\big)_e\\&\quad\le C\|(\boldsymbol{K}_i^{-1}\boldsymbol{u}_h^i+\nabla p_h^i)\cdot\boldsymbol{\tau}\|_{0,e}\left(h_e^{-\frac{1}{2}}\|\boldsymbol{K}_i^{-1}(\boldsymbol{u}_i-\boldsymbol{u}_h^i)\|_{0,T_e}+h_e^{\frac{1}{2}}\|\mathrm{curl}\,(\boldsymbol{K}_i^{-1}\boldsymbol{u}_h^i)\|_{0,T_e}\right).\end{aligned}$$

Since $B_e=0$ on ∂e, by integration by parts, we have

$$\begin{aligned}&\big(B_e(\boldsymbol{K}_i^{-1}\boldsymbol{u}_h^i+\nabla p_h^i)\cdot\boldsymbol{\tau},(\nabla p_h^i-\nabla p_i)\cdot\boldsymbol{\tau}\big)_e\\&\quad=\left(\frac{d\big(B_e(\boldsymbol{K}_i^{-1}\boldsymbol{u}_h^i+\nabla p_h^i)\cdot\boldsymbol{\tau}\big)}{d\boldsymbol{s}},p_i-p_h^i\right)_e\\&\quad\le Ch_e^{-1}\|(\boldsymbol{K}_i^{-1}\boldsymbol{u}_h^i+\nabla p_h^i)\cdot\boldsymbol{\tau}\|_{0,e}\|p_i-p_h^i\|_{0,e}.\end{aligned}$$

Hence, by (4.1), we can further deduce that

$$Ch_e^2\|(\boldsymbol{K}_i^{-1}\boldsymbol{u}_h^i+\nabla p_h^i)\cdot\boldsymbol{\tau}\|_{0,e}^2\le h_e\|\boldsymbol{K}_i^{-1}(\boldsymbol{u}_i-\boldsymbol{u}_h^i)\|_{0,T_e}^2+\|p_i-p_h^i\|_{0,e}^2.\quad(4.6)$$

For $i=1,2$, noting that $\|p_i-p_h^i\|_{0,e}=\|\{p-p_h\}_\gamma+(-1)^{i-1}\frac{1}{2}[\![p-p_h]\!]_\gamma\|_{0,e}$, then by the Eqs. (2.2e) and (2.2f), we deduce that

$$\begin{aligned}&\|\{p-p_h\}_\gamma\|_{0,e}\\&\quad=\|\widehat{p}_\gamma+\xi_\gamma\eta_\gamma[\![\boldsymbol{u}\cdot\boldsymbol{n}]\!]_\gamma-(\widehat{p}_h^\gamma+\xi_\gamma\eta_\gamma[\![\boldsymbol{u}_h\cdot\boldsymbol{n}]\!]_\gamma)+(\widehat{p}_h^\gamma+\xi_\gamma\eta_\gamma[\![\boldsymbol{u}_h\cdot\boldsymbol{n}]\!]_\gamma)-\{p_h\}_\gamma\|_{0,e}\\&\quad\le\|\widehat{p}_\gamma-\widehat{p}_h^\gamma\|_{0,e}+\xi_\gamma\eta_\gamma\|[\![(\boldsymbol{u}-\boldsymbol{u}_h)\cdot\boldsymbol{n}]\!]_\gamma\|_{0,e}+\|\{p_h\}_\gamma-\widehat{p}_h^\gamma-\xi_\gamma\eta_\gamma[\![\boldsymbol{u}_h\cdot\boldsymbol{n}]\!]_\gamma\|_{0,e}\end{aligned}$$

and

$$\begin{aligned}\|[\![p-p_h]\!]_\gamma\|_{0,e}&=\|\eta_\gamma\{\boldsymbol{u}\cdot\boldsymbol{n}\}_\gamma-\eta_\gamma\{\boldsymbol{u}_h\cdot\boldsymbol{n}\}_\gamma+\eta_\gamma\{\boldsymbol{u}_h\cdot\boldsymbol{n}\}_\gamma-[\![p_h]\!]_\gamma\|_{0,e}\\&\le\eta_\gamma\|\{(\boldsymbol{u}-\boldsymbol{u}_h)\cdot\boldsymbol{n}\}_\gamma\|_{0,e}+\|[\![p_h]\!]_\gamma-\eta_\gamma\{\boldsymbol{u}_h\cdot\boldsymbol{n}\}_\gamma\|_{0,e}.\end{aligned}$$

Now we can conclude the desired result by (4.6), the above two estimates for $\|p_i-p_h^i\|_{0,e}$, the Eqs. (2.2e) and (2.2f), and (3.16).

Lemma 4.6 *For any $e\in\mathcal{T}_h^\gamma$, there holds*

$$\eta_{e,\gamma,2}\le\|\nabla_{\boldsymbol{\tau}}\cdot(\widehat{\boldsymbol{u}}_\gamma-\widehat{\boldsymbol{u}}_h^\gamma)\|_{0,e}+\sum_{i=1}^2\|(\boldsymbol{u}_i-\boldsymbol{u}_h^i)\cdot\boldsymbol{n}\|_{0,e}.$$

Proof The desired estimate directly follows from the Eq. (2.2c) and the triangular inequality.

Lemma 4.7 *For any $e\in\mathcal{T}_h^\gamma$, there holds*

$$C\eta_{e,\gamma,3}\le h_e\widehat{\eta}_\gamma\|\widehat{\boldsymbol{u}}_\gamma-\widehat{\boldsymbol{u}}_h^\gamma\|_{0,e}+\|\widehat{p}_\gamma-\widehat{p}_h^\gamma\|_{0,e}.$$

Proof We apply the property of bubble function B_e and the Eq. (2.2d) to obtain

$$\begin{aligned}
&\|(\widehat{\eta}_\gamma \widehat{\boldsymbol{u}}_h^\gamma + \nabla_{\boldsymbol{\tau}} \widehat{p}_h^\gamma)\cdot\boldsymbol{\tau}\|_{0,e}^2 \\
&\le C\big(B_e(\widehat{\eta}_\gamma \widehat{\boldsymbol{u}}_h^\gamma + \nabla_{\boldsymbol{\tau}} \widehat{p}_h^\gamma)\cdot\boldsymbol{\tau}, (\widehat{\eta}_\gamma \widehat{\boldsymbol{u}}_h^\gamma + \nabla_{\boldsymbol{\tau}} \widehat{p}_h^\gamma)\cdot\boldsymbol{\tau} - (\widehat{\eta}_\gamma \widehat{\boldsymbol{u}}_\gamma + \nabla_{\boldsymbol{\tau}} \widehat{p}_\gamma)\cdot\boldsymbol{\tau}\big)_e \\
&\le C\|(\widehat{\eta}_\gamma \widehat{\boldsymbol{u}}_h^\gamma + \nabla_{\boldsymbol{\tau}} \widehat{p}_h^\gamma)\cdot\boldsymbol{\tau}\|_{0,e}\widehat{\eta}_\gamma\|\widehat{\boldsymbol{u}}_\gamma - \widehat{\boldsymbol{u}}_h^\gamma\|_{0,e} \\
&\quad + C\left(\frac{d(B_e(\widehat{\eta}_\gamma \widehat{\boldsymbol{u}}_h^\gamma + \nabla_{\boldsymbol{\tau}} \widehat{p}_h^\gamma)\cdot\boldsymbol{\tau})}{d\boldsymbol{s}}, \widehat{p}_\gamma - \widehat{p}_h^\gamma\right)_e \\
&\le C\|(\widehat{\eta}_\gamma \widehat{\boldsymbol{u}}_h^\gamma + \nabla_{\boldsymbol{\tau}} \widehat{p}_h^\gamma)\cdot\boldsymbol{\tau}\|_{0,e}\widehat{\eta}_\gamma\|\widehat{\boldsymbol{u}}_\gamma - \widehat{\boldsymbol{u}}_h^\gamma\|_{0,e} \\
&\quad + Ch_e^{-1}\|(\widehat{\eta}_\gamma \widehat{\boldsymbol{u}}_h^\gamma + \nabla_{\boldsymbol{\tau}} \widehat{p}_h^\gamma)\cdot\boldsymbol{\tau}\|_{0,e}\|\widehat{p}_\gamma - \widehat{p}_h^\gamma\|_{0,e},
\end{aligned}$$

which immediately implies the desired result.

Now the estimate (2.9) in Theorem 2.1 directly follows from Lemmas 4.2–4.7 and the definition of $\eta_{\partial\gamma^D}$.

5 Numerical experiments

In this section, we present numerical results based on the application of adaptive mixed finite element method (AMFEM) for the reduced model (2.2) of single-phase Darcy flow in fractured porous media to show how the meshes are generated adaptively and how the a posteriori error estimator behaves due to effects from the fractures, the lack of regularity of solution and different domains. We both choose polynomial degree $k = 1$ for the Raviart–Thomas mixed finite element space for discrete velocity and Q_h for discrete pressure in the following experiments. The procedure of the AMFEM consists of adaptive loops of the cycle 'Solve → Estimate → Mark → Refine'. We utilize the direct method in the 'Solve' step to solve the discrete algebraic system. In the step 'Refine', we apply the a posteriori error estimator proposed in this paper. We adopt the newest vertex bisection algorithm (cf. [37] and the references therein) in the step 'Refine'. In the step 'Mark', we use the bulk algorithm. Let $\mathcal{M}_h^F$ be the set of marked edges such that

$$\begin{aligned}
&\sum_{i=1}^{2}\left(\sum_{e\in\mathcal{M}_h^F\cap\mathcal{E}_h^0(\Omega_i)}\eta_e^2 + \sum_{e\in\mathcal{M}_h^F\cap\mathcal{E}_h(\Gamma_i^D)}\eta_{e,\Gamma_i^D}^2\right) + \sum_{e\in\mathcal{M}_h^F\cap\mathcal{T}_h^\gamma}\eta_{e,\gamma}^2 + \sum_{e_d\in\mathcal{M}_h^F}\eta_{\partial\gamma^D}^2 \\
&\ge \theta_1\left(\sum_{i=1}^{2}\left(\sum_{e\in\mathcal{E}_h^0(\Omega_i)}\eta_e^2 + \sum_{e\in\mathcal{E}_h(\Gamma_i^D)}\eta_{e,\Gamma_i^D}^2\right) + \sum_{e\in\mathcal{T}_h^\gamma}\eta_{e,\gamma}^2 + \eta_{\partial\gamma^D}^2\right).
\end{aligned}$$

Let $\mathcal{M}_h^T$ be the set of triangles with one edge in $\mathcal{M}_h^F$, then we enlarge $\mathcal{M}_h^T$ such that

$$\sum_{T\in\mathcal{M}_h^T}\eta_T^2 \ge \theta_2\sum_{i=1}^{2}\sum_{T\in\mathcal{T}_h^i}\eta_T^2.$$

Here θ_1 and θ_2 are adjustable parameters. The numerical implementation is based on the FFW toolbox [12]. We set $\theta_1 = \theta_2 = 0.5$. In the following examples, we assume that the data g^D on the Dirichlet boundary are always constant. Thus, we can avoid the 'Mark' step for the oscillation terms of data which vanish here. We choose the parameter ξ in the reduced model (2.2) as $\xi = 3/4$ and assume that the thickness of fracture is always 0.01 in our experiments. The source term is set to be zero and the permeability in the surrounding porous media is always assumed to be $\boldsymbol{K} = \mathbf{Id}$ in the following examples, where $\mathbf{Id}$ is the two-dimensional identity matrix.

Although the boundary condition is discussed as in (2.3) in this paper, similar results are valid for other types of boundary conditions as well. In the following the approximate velocity is plotted based on $\widehat{\boldsymbol{u}}_h^{\gamma} + \widehat{\boldsymbol{u}}_{\gamma,h}^{\boldsymbol{n}}$, where $\widehat{\boldsymbol{u}}_{\gamma,h}^{\boldsymbol{n}}$ is the approximate normal component of Darcy velocity $\widehat{\boldsymbol{u}}_{\gamma}^{\boldsymbol{n}}$ in the fracture (cf. Remark 1). The figures displaying the convergence history of the a posteriori error estimator are all plotted in log-log coordinates.

Now we first present examples for the problems with non-intersecting fractures.

Example 5.1 We consider the reduced model (2.2) in the domain $\Omega = [0, 2] \times [0, 1]$ with only one reduced fracture γ on the line $\{1\} \times [0, 1]$. Let $\Omega_1 = [0, 1] \times [0, 1]$ and $\Omega_2 = [1, 2] \times [0, 1]$. In the first case, we consider the reduced model (2.2) with exact pressure solutions $p|_{\Omega_1} = y + \frac{1}{2}\tanh(\frac{x-1}{\alpha}) + \frac{1}{2}$, $p|_{\Omega_2} = y + \frac{1}{2}\tanh(\frac{x-1}{2\alpha}) + \frac{1}{2} + \frac{3\eta_\gamma}{8\alpha}$, $\widehat{p}_\gamma = y + \frac{1}{2} + \frac{3\eta_\gamma}{16\alpha} + \frac{\xi_\gamma \eta_\gamma}{4\alpha}$, where α is an optional parameter. The permeability in the fracture is given by $\boldsymbol{K}_f = 100\mathbf{Id}$. The Dirichlet boundary conditions hold on the fracture boundaries and part of surrounding porous media boundary $\{2\} \times [0, 1] \cup \{0\} \times [0, 1]$, and Neumann boundary condition is imposed on the remaining part of $\partial\Omega$.

In the second case, we consider the reduced model (2.2) without exact solutions. The permeability in the fracture is given by $\boldsymbol{K}_f = K_f\mathbf{Id}$, where $K_f = 200$ on $L_1 = \{1\} \times ([0, 1/4] \cup [3/4, 1])$ and $K_f = 0.001$ on $L_2 = \{1\} \times [1/4, 3/4]$. We assume that homogeneous Neumann boundary conditions hold on the fracture boundaries. For the surrounding porous media, the Dirichlet boundary condition is given by $p = 1$ on $\{2\} \times [0, 1]$ and $p = 0$ on $\{0\} \times [0, 1]$, and the other part of $\partial\Omega$ is homogeneous Neumann boundary condition.

We choose the initial quasi-uniform mesh consisting of 16 triangles and the initial mesh size $h_0 = 1/2$ for both cases in this example. For the first case, Fig. 2 displays the adaptively refined mesh by 10 iterations of the AMFEM and the approximate pressure p_h^* by 17 iterations for the problem with $\alpha = 0.01$. We can see that the mesh is locally refined near the fracture γ due to the fact that a transition layer is introduced for the pressure p near γ. Figure 3 shows the convergence history of the a posteriori error estimator η and the total energy error $|||(\boldsymbol{u}^* - \boldsymbol{u}_h^*, p^* - p_h^*)|||_h$ as a function of the total number of triangles N on adaptively refined meshes for the problems with $\alpha = 0.1$ and 0.01. The convergence results indicate the almost optimal convergence rate $O(N^{-1})$ of the a posteriori error estimator η and the total energy error for both two cases.

For the second case, Fig. 4 displays the adaptively refined mesh and the corresponding approximate pressure p_h^* by 10 iterations of the AMFEM. The associated approximate velocity $\boldsymbol{u}_h^*$ in the fracture and the surrounding porous media is shown in

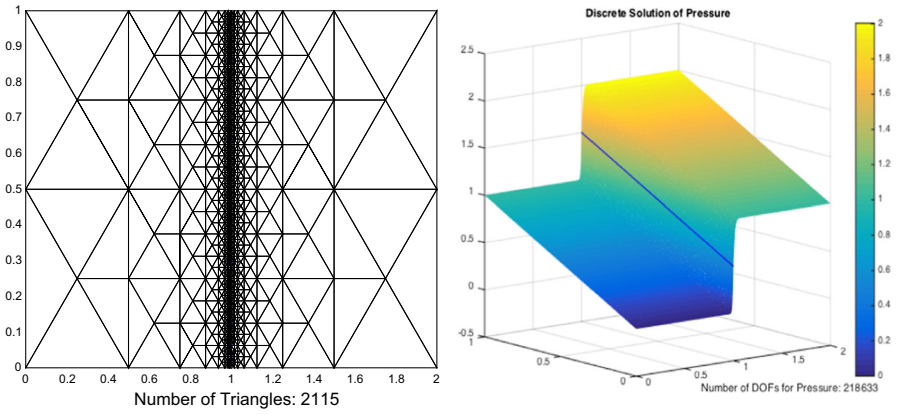

Fig. 2 (The first case of Example 5.1 with $\alpha = 0.01$) *Left* Adaptively refined mesh. *Right* 3D plot of the corresponding approximate pressure p_h^*

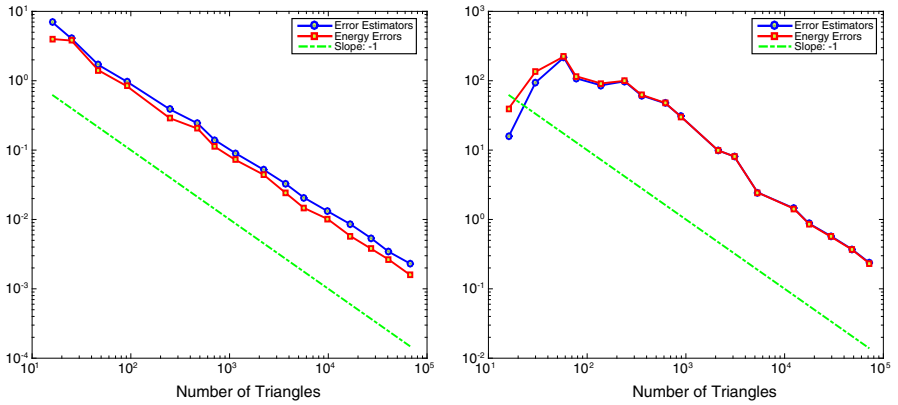

Fig. 3 (The first case of Example 5.1) Convergence history of the a posteriori error estimator η and the total energy error $|||(\boldsymbol{u}^* - \boldsymbol{u}_h^*, p^* - p_h^*)|||_h$. *Left* $\alpha = 0.1$. *Right* $\alpha = 0.01$

the left graph of Fig. 5. One can observe that the mesh is always locally refined near the ends of L_2. Indeed, the permeability of fracture admits changes across the ends of L_2 and L_2 represents a barrier due to the small permeability. The pressure appears discontinuity across L_2. The right graph in Fig. 5 shows the a posteriori error estimator η as a function of the total number of triangles N on adaptively refined meshes and quasi-uniform meshes. The convergence results indicate the almost optimal convergence rate $O(N^{-1})$ of the a posteriori error estimator η which is faster than that on the quasi-uniform meshes.

Example 5.2 We consider the reduced model (2.2) in the L-shaped domain $\Omega = ([0, 2] \times [-1, 1])\backslash([0, 1] \times [-1, 0])$. The reduced fracture lies on the polygonal line $L_1 \cup L_2 \cup L_3$, where $L_1 = (\{1/2\} \times [1/2, 1]) \cup ([1/2, 1] \times \{1/2\})$, $L_2 = ([1, 3/2] \times \{1/2\}) \cup (\{3/2\} \times [0, 1/2])$ and $L_3 = \{3/2\} \times [-1, 0]$. The permeability in the fracture is given by $\boldsymbol{K}_f = K_f \mathbf{Id}$, where $K_f = 100$ on $L_1 \cup L_3$ and $K_f = 0.01$ on L_2. For

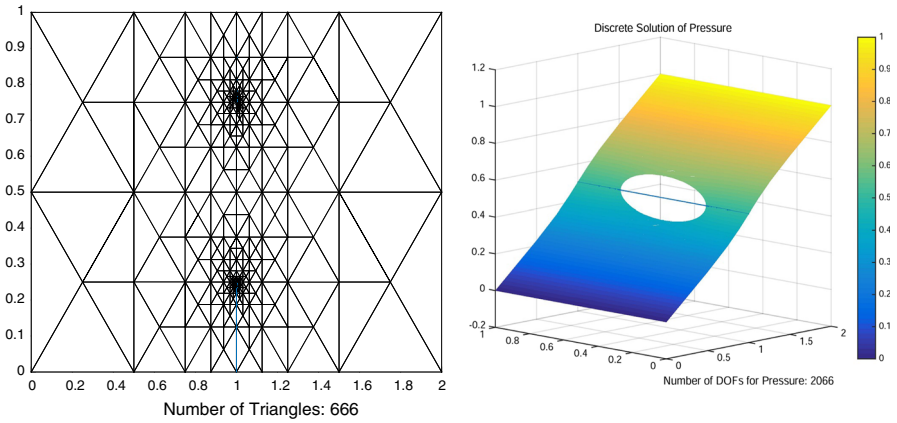

Fig. 4 (The second case of Example 5.1) *Left* Adaptively refined mesh. *Right* 3D plot of the corresponding approximate pressure p_h^*

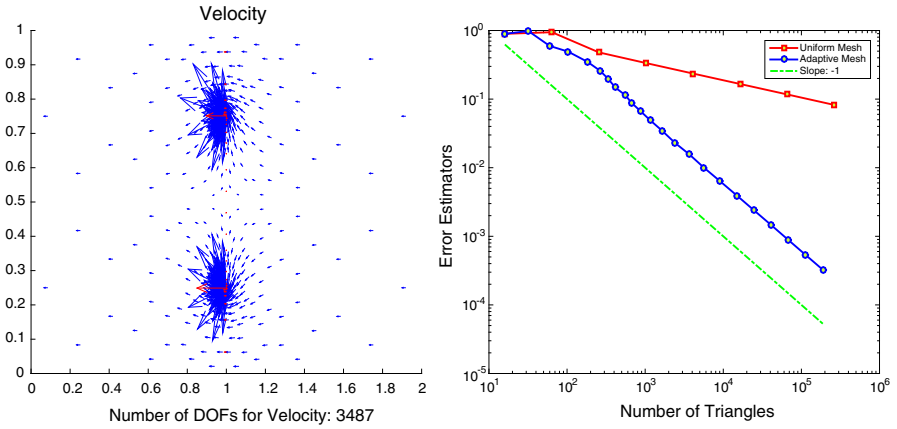

Fig. 5 (The second case of Example 5.1) *Left* Approximate velocity $\boldsymbol{u}_h^*$ based on the adaptively refined mesh as in Fig. 4. *Right* Convergence history of the a posteriori error estimator η

the surrounding porous media, the Dirichlet boundary condition is given by $p = 1$ on $[0, 2] \times \{1\}$ and $p = 0$ on $[1, 2] \times \{-1\}$, and homogeneous Neumann boundary condition is imposed on the other part of $\partial\Omega$. Dirichlet boundary conditions hold on the fracture boundaries as $\widehat{p}_\gamma = 1$ at the end point $(1/2, 1)$ and $\widehat{p}_\gamma = 0$ at another end point $(3/2, -1)$.

The initial mesh is chosen to be composed of 24 triangles with initial mesh size $h_0 = 1/2$. Figure 6 displays the adaptively refined mesh and the corresponding approximate velocity $\boldsymbol{u}_h^*$ by 10 iterations of the AMFEM. Figure 7 shows the adaptively refined mesh and the associated approximate pressure p_h^* by 13 iteration of the AMFEM. One can observe that the mesh starts to be locally refined near the corner point $(1, 0)$, the two end points and corner point $(3/2, 1/2)$ of L_2. On the fine mesh, the mesh is further to be locally refined near the corner point $(1, 0)$ and around the reduced fracture. The

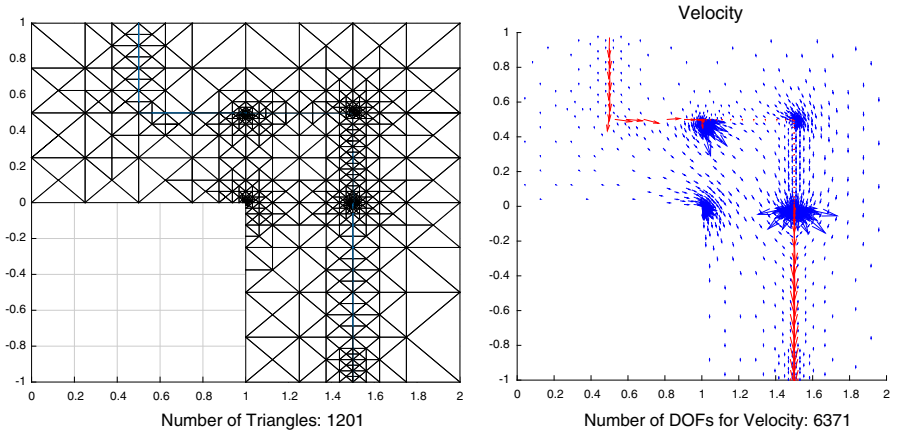

Fig. 6 (Example 5.2) *Left* Adaptively refined mesh. *Right* The corresponding approximate velocity $\boldsymbol{u}_h^*$

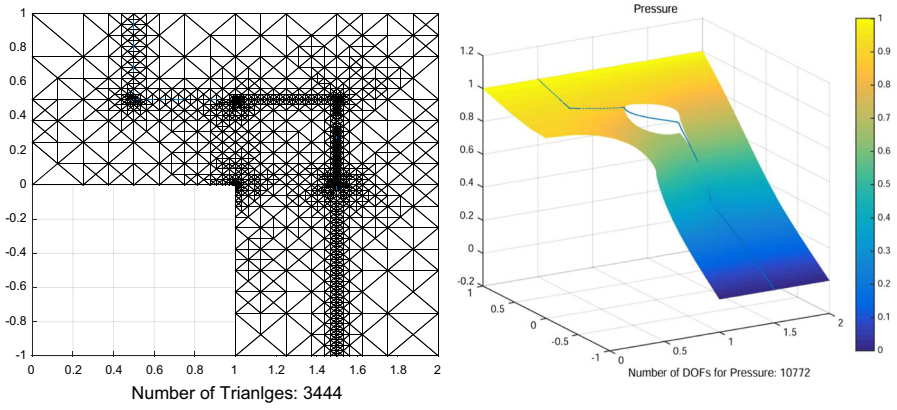

Fig. 7 (Example 5.2) *Left* Adaptively refined mesh. *Right* 3D plot of the corresponding approximate pressure p_h^*

pressure discontinuity across L_2 is observed due to the small permeability in L_2. From Fig. 8, the optimal convergence rate $O(N^{-1})$ of the a posteriori error estimator η in the AMFEM is also observed.

Example 5.3 We consider the reduced model (2.2) with more non-intersecting fractures totally or partially immersed in the porous media. Ω is a L-shaped domain as in Example 5.2. The reduced fractures lie on the lines L_1, L_2, L_3 and L_4, where $L_1 = [1/2, 1] \times \{1/2\}$, $L_2 = \{3/2\} \times [1/2, 1]$, $L_3 = [3/2, 2] \times \{0\}$ and $L_4 = \{3/2\} \times [-1, -\frac{1}{2}]$. The permeability in the fractures is given by $\boldsymbol{K}_f = K_f \mathbf{Id}$, where $K_f = 100$ on L_1 and L_4, $K_f = 0.01$ on L_2 and L_3. For the surrounding porous media, the Dirichlet boundary condition is given by $p = 1$ on $0 \times [0, 1]$ and $p = 0$ on $[1, 2] \times \{-1\}$, and homogeneous Neumann boundary condition is imposed on the other part of $\partial\Omega$. Homogeneous boundary conditions hold on the fracture boundaries except

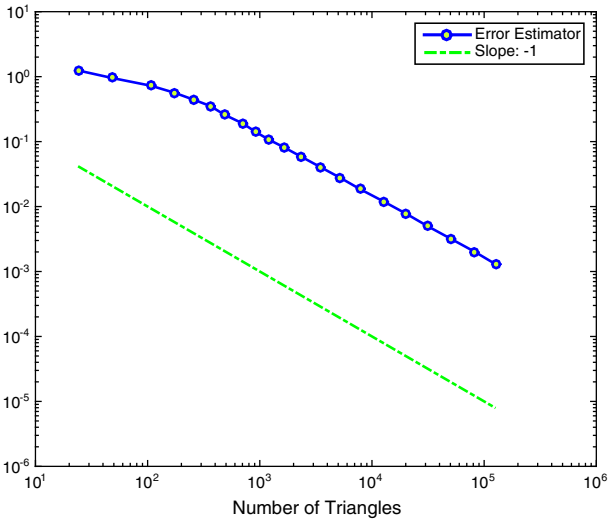

Fig. 8 (Example 5.2) Convergence history of the a posteriori error estimator η

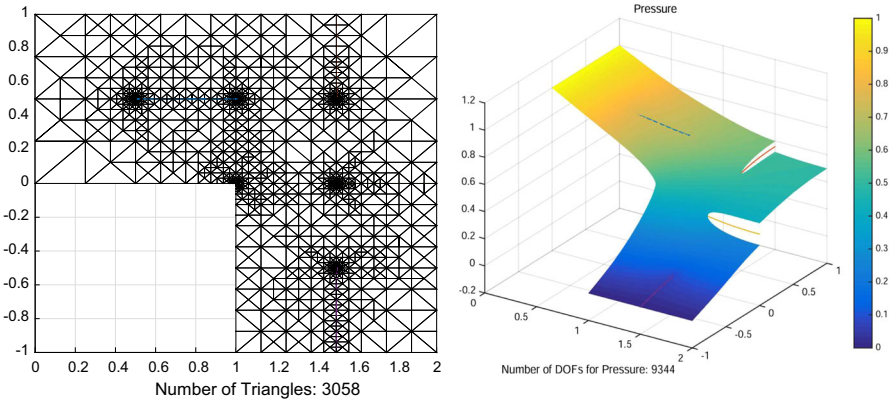

Fig. 9 (Example 5.3) *Left* Adaptively refined mesh. *Right* 3D plot of the corresponding approximate pressure p_h^*

the end point $(3/2, -1)$ which is imposed by the homogeneous Dirichlet boundary condition.

The initial mesh is chosen as in Example 5.2. Figure 9 shows the adaptively refined mesh and the associated approximate pressure p_h^* by 13 iterations of the AMFEM. The corresponding approximate velocity $\boldsymbol{u}_h^*$ is shown in the left graph of Fig. 10. The mesh is locally refined at the corner point $(1, 0)$ and the interior end points of the fractures. Since the permeabilities in L_2 and L_3 are small, the pressure admits discontinuity across L_2 and L_3. The right graph of Fig. 10 also indicates the optimal convergence rate $O(N^{-1})$ of the a posteriori error estimator η in the AMFEM.

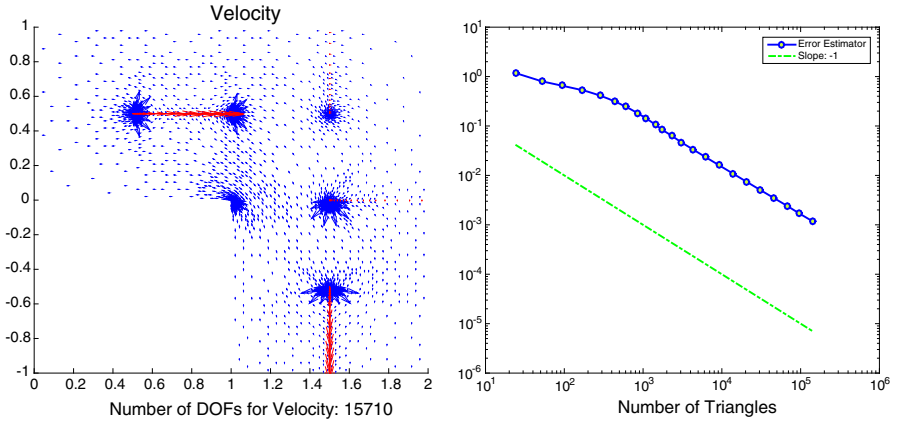

Fig. 10 (Example 5.3) *Left* Approximate velocity $\boldsymbol{u}_h^*$ based on the adaptively refined mesh as in Fig. 9. *Right* Convergence history of the a posteriori error estimator η

Next, we present an example for the problem with intersecting fractures. In this case, besides the interface conditions across the fractures mentioned in (2.2), the reduced model should also be coupled with additional coupling conditions at the intersection points for the fracture-fracture system (cf. [21,23]). For simplicity, we assume there are only two intersecting fracture subdomains $\Omega_{f,1}$ and $\Omega_{f,2}$ in the fractured porous media Ω. For $i = 1, 2$, let d_i denote the thickness of fracture $\Omega_{f,i}$, and the fracture subdomains $\Omega_{f,i}$ can be reduced as a polygonal line γ_i. Let $I = \Omega_{f,1} \cap \Omega_{f,2}$ and $\boldsymbol{i}_p = \gamma_1 \cap \gamma_2$. Then we set $\gamma_i = \gamma_{i,1} \cup \gamma_{i,2}$, $\gamma_{i,1} \cap \gamma_{i,2} = \boldsymbol{i}_p$, $i = 1, 2$. The Darcy flow in the intersection subdomain I is governed by $\nabla \cdot \boldsymbol{u}_I = q_I$ and $\boldsymbol{u}_I = -\boldsymbol{K}_I \nabla p_I$. For $i = 1, 2$, we denote by $\boldsymbol{\tau}_i$ the unit tangential vector along γ_i with $\boldsymbol{\tau}_{i,\boldsymbol{i}_p} = \boldsymbol{\tau}_i|_{\boldsymbol{i}_p}$, and define $\eta_{ij}^I = (\boldsymbol{K}_I^{-1}\boldsymbol{\tau}_{i,\boldsymbol{i}_p}, \boldsymbol{\tau}_{j,\boldsymbol{i}_p})$ and $d_i^* = d_i / \sin\theta$, where $\theta = \arccos \boldsymbol{\tau}_{1,\boldsymbol{i}_p} \cdot \boldsymbol{\tau}_{2,\boldsymbol{i}_p}$. In the reduced model we assume $\widehat{\boldsymbol{u}}_{\gamma_i}$ and $\widehat{p}_{\gamma_i}$ are reduced velocity and pressure on γ_i respectively. The reduced pressures $\widehat{p}_{\gamma_1}$ and $\widehat{p}_{\gamma_2}$ may be discontinuous at the intersection point $\boldsymbol{i}_p$. Let $[\![a_i]\!]_{\boldsymbol{i}_p} = a_{i,1}|_{\boldsymbol{i}_p} - a_{i,2}|_{\boldsymbol{i}_p}$. The coupling condition at the intersection point $\boldsymbol{i}_p$ has been proposed in [21,23] as follows:

$$
\begin{aligned}
&\frac{|I|}{d_i} \sum_{j=1}^{2} \frac{\eta_{ij}^I}{d_j^*} \{\widehat{\boldsymbol{u}}_{\gamma_j} \cdot \boldsymbol{\tau}_j\}_{\boldsymbol{i}_p} = [\![\widehat{p}_{\gamma_i}]\!]_{\boldsymbol{i}_p}, \quad i = 1, 2,\\
&\widehat{\xi}_I \frac{d_j}{d_i} \eta_{ii}^I [\![\widehat{\boldsymbol{u}}_{\gamma_i} \cdot \boldsymbol{\tau}_i]\!]_{\boldsymbol{i}_p} = \{\widehat{p}_{\gamma_i}\}_{\boldsymbol{i}_p} - \widehat{p}_I, \quad i, j = 1, 2,\ i \neq j,\\
&\sum_{j=1}^{2} [\![\widehat{\boldsymbol{u}}_{\gamma_j} \cdot \boldsymbol{\tau}_j]\!]_{\boldsymbol{i}_p} = \widehat{q}_I,
\end{aligned}
$$

where $\widehat{p}_I = \frac{1}{|I|}\int_I p_I$, $\widehat{q}_I = \int_I q_I$ and $\widehat{\xi}_I = (2\xi_I - 1)/4$ with $\xi_I > 1/2$. Combining the reduced model (2.2) and the above coupling condition at the intersection point yields the complete reduced model for the problem with intersecting fractures. The

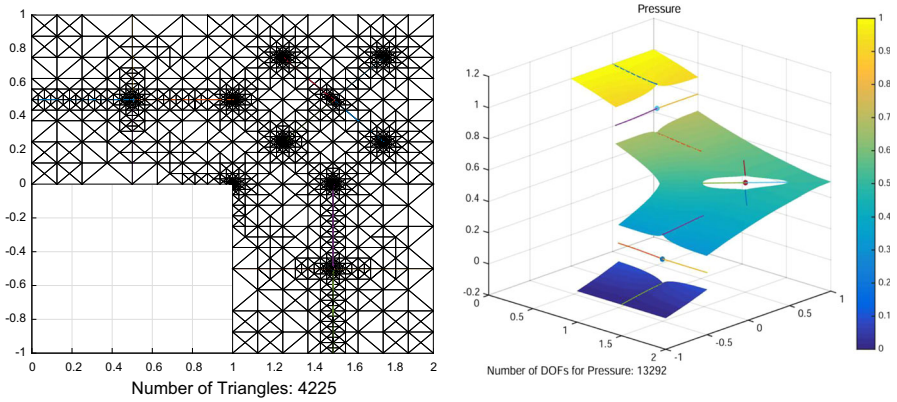

Fig. 11 (Example 5.4) *Left* Adaptively refined mesh. *Right* 3D plot of the corresponding approximate pressure p_h^*

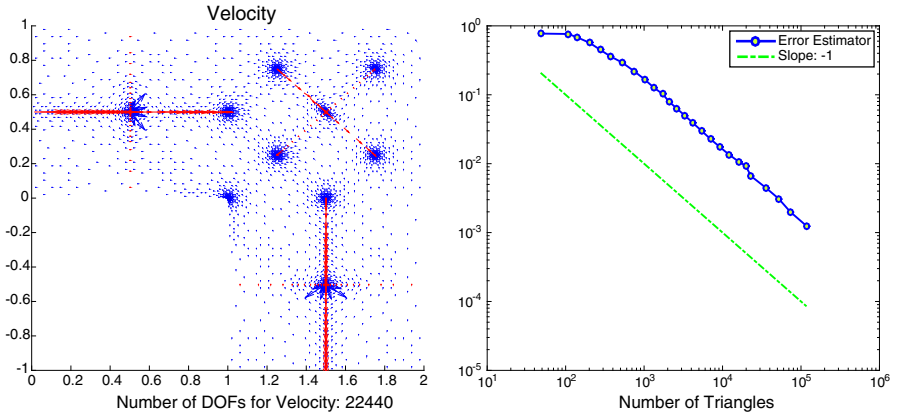

Fig. 12 (Example 5.4) *Left* Approximate velocity $\boldsymbol{u}_h^*$ based on the adaptively refined mesh as in Fig. 11. *Right* Convergence history of the a posteriori error estimator η

corresponding weak formulation can also be written (cf. [23]) and solved by the AMFEM.

Example 5.4 We consider the reduced model mentioned above for the single-phase Darcy flow in the fractured porous media with intersecting fractures. The domain Ω and the boundary conditions for the flow in the surrounding porous media are chosen as the same in Example 5.3. The reduced fractures lie on the lines L_1, L_2, L_3, L_4, L_5 and L_6, where $L_1 = [0, 1] \times \{1/2\}$, $L_2 = \{1/2\} \times [0, 1]$, $L_3 = \{(x, y) : \ y = 2 - x, \ y \in [1/4, 3/4]\}$, $L_4 = \{(x, y) : \ y = x - 1, \ y \in [1/4, 3/4]\}$, $L_5 = \{3/2\} \times [-1, 0]$, $L_6 = [1, 2] \times \{-1/2\}$. The permeability in the fractures is given by $\boldsymbol{K}_f = K_f \mathbf{Id}$, where $K_f = 100$ on L_1, L_3 and L_5, $K_f = 0.01$ on L_2, L_4 and L_6. The permeability is given by $\boldsymbol{K}_I = K_I \mathbf{Id}$ at the intersection points $\boldsymbol{i}_{p_1} = (1/2, 1/2)$, $\boldsymbol{i}_{p_2} = (3/2, 1/2)$ and $\boldsymbol{i}_{p_3} = (3/2, -1/2)$, where $K_I = 0.01$. Homogeneous boundary conditions hold

on the fracture boundaries except the end points $(0, 1/2)$ and $(3/2, -1)$ which are imposed by $\widehat{p}_\gamma = 1$ and $\widehat{p}_\gamma = 0$ respectively.

The initial mesh is chosen as in Example 5.2. We choose the parameter $\xi_I = 3/4$ in the coupling conditions at the intersection points. Figure 11 displays the adaptively refined mesh and the associated approximate pressure p_h^* by 15 iterations of the AMFEM. The associated approximate velocity $\boldsymbol{u}_h^*$ is shown in the left graph of Fig. 12. One can observe that the mesh is locally refined near the corner point $(1, 0)$, the interior end points of the fractures and the intersection points. Due to the small permeability in L_2, L_4 and L_6, the pressure admits discontinuity across these three reduced fractures. The right graph of Fig. 12 implies the optimal convergence rate $O(N^{-1})$ of the a posteriori error estimator η in the AMFEM.

6 Conclusion

We develop a robust a posteriori error estimator for the Raviart–Thomas mixed finite element method for single-phase Darcy flow in a two-dimensional fractured porous media. The DFM is used to model the flow in the fracture by a one-dimensional problem. The reliability and efficiency of the a posteriori error estimator are established for the problem with single fracture. The key contribution in the analysis lies in the coupling of error estimates between one and two dimensions. Proper interface conditions across the fracture play an important role in the analysis to relate the one-dimensional flow in the fracture and the two-dimensional flow in the surrounding porous media. To our best knowledge, it is the first time that a robust a posteriori error estimator is given for the reduced model of single-phase Darcy flow based on the DFM in the fractured porous media. From numerical results we find that the a posteriori error estimator works well for the problems with non-intersecting fractures and with intersecting fractures. The future work of interest includes the extension of our analysis to the problem with intersecting fractures in the two and three dimensional fractured porous media and the development of the corresponding numerical implementation.

Acknowledgements The authors are very grateful to the anonymous referees for their valuable comments and suggestions that led to an improved presentation of this paper.

References

1. Achdou, Y., Bernardi, C., Coquel, F.: A priori and a posteriori analysis of finite volume discretizations of Darcy's equations. Numer. Math. **96**, 17–42 (2003)
2. Adams, R.: Sobolev Spaces. Academic Press, New York (1975)
3. Ainsworth, M., Oden, J.T.: A Posteriori Error Estimation in Finite Element Analysis. Wiley, New York (2000)
4. Ainsworth, M.: A posteriori error estimation for lowest order Raviart–Thomas mixed finite elements. SIAM J. Numer. Anal. **30**, 189–204 (2007)
5. Alboin, C., Jaffré, J., Roberts, J.E., Serres, C.: Modeling fractures as interfaces for flow and transport in porous media. In: Fluid Flow and Transport in Porous Media: Mathematical and Numerical Treatment (South Hadley, MA, 2001). Contemporary Mathematics, vol. 295, pp. 13–24 (2002)
6. Babuška, I., Gatica, G.N.: A residual-based a posteriori error estimator for the Stokes–Darcy coupled problem. SIAM J. Numer. Anal. **48**, 498–523 (2010)

7. Barenblatt, G., Zheltov, Y., Kochina, I.: Basic concepts in the theory of seepage of homogeneous fluids in fissured rocks. J. Appl. Math. Mech. **24**, 1286–1303 (1960)
8. Baca, R., Arnett, R., Langford, D.: Modeling fluid flow in fractured porous rock masses by finite element techniques. Int. J. Num. Methods Fluids **4**, 337–348 (1984)
9. Barrios, T.P., Bustinza, R.: An a posteriori error analysis of an augmented discontinuous Galerkin formulation for Darcy flow. Numer. Math. **120**, 231–269 (2012)
10. Braess, D., Verfürth, R.: A posteriori error estimators for the Raviart–Thomas element. SIAM J. Numer. Anal. **33**, 2431–2444 (1996)
11. Brezzi, F., Fortin, M.: Mixed and Hybrid Finite Element Methods. Springer, New York (1991)
12. Byfut, A., Gedicke, J., Günther, D., Reininghaus, J., Wiedemann, S., et al.: FFW Documentation. Humboldt University of Berlin, Germany (2007)
13. Cai, Z., Zhang, S.: Recovery-based error estimators for interface problems: mixed and nonconforming finite elements. SIAM J. Numer. Anal. **48**, 30–52 (2010)
14. Cai, J., Sun, S.: Fractal analysis of fracture increasing spontaneous imbibition in porous media saturated with gas. Int. J. Mod. Phys. C **24**, 1350056 (2013)
15. Carstensen, C.: A posteriori error estimate for the mixed finite element method. Math. Comput. **66**, 465–476 (1997)
16. Chen, H., Salama, A., Sun, S.: Adaptive mixed finite element methods for Darcy flow in fractured porous media. Water Resour. Res. (2016). doi:10.1002/2015WR018450
17. Dawson, C., Sun, S., Wheeler, M.F.: Compatible algorithms for coupled flow and transport. Comput. Methods Appl. Mech. Eng. **193**, 2565–2580 (2004)
18. Demkowicz, L.: Polynomial Exact Sequences and Projection-Based Interpolation with Application to Maxwell Equations. Lecture Notes in Mathematics. Springer, Berlin (2008)
19. Dong, C., Sun, S., Taylor, G.A.: Numerical modeling of contaminant transport in fractured porous media using mixed finite element and finite volume methods. J. Porous Media. **14**, 219–242 (2011)
20. Ervin, V.J., Jenkins, E.W., Sun, S.: Coupled generalized non-linear stokes flow with flow through a porous medium. SIAM J. Numer. Anal. **47**, 929–952 (2009)
21. Formaggia, L., Fumagalli, A., Scotti, A., Ruffo, P.: A reduced model for Darcy's problem in networks of fractures. ESAIM Math. Model. Numer. Anal. **48**, 1089–1116 (2014)
22. Frih, N., Roberts, J.E., Saada, A.: Modeling fractures as interfaces: a model for Forchheimer fractures. Comput. Geosci. **12**, 91–104 (2008)
23. Fumagalli, A.: Numerical Modelling of Flows in Fractured Porous Media by the XFEM Method. Ph.D. thesis. Politecnico di Milano (2012)
24. Gebauer, S., Neunhäuserer, L., Kornhuber, R., Ochs, S., Hinkelmann, R., Helmig, R.: Equidimensional modelling of flow and transport processes in fractured porous systems I. Dev. Water Sci. **47**, 335–342 (2002)
25. Girault, V., Raviart, P.A.: Finite Element Methods for Navier–Stokes Equations: Theory and Algorithms. Springer, Berlin (1986)
26. Gopalakrishnan, J., Qiu, W.: Partial expansion of a Lipschitz domain and some applications. Front. Math. China **7**, 249–272 (2012)
27. Hoteit, H., Firoozabadi, A.: Multicomponent fluid flow by discontinuous Galerkin and mixed methods in unfractured and fractured media. Water Resour. Res. **41**, W11412 (2005)
28. Hoteit, H., Firoozabadi, A.: An efficient numerical model for incompressible two-phase flow in fractured media. Adv. Water Resour. **31**, 891–905 (2008)
29. Kim, K.: A posteriori error analysis for locally conservative mixed methods. Math. Comput. **76**, 43–66 (2007)
30. Lovadina, C., Stenberg, R.: Energy norm a posteriori error estimates for mixed finite element methods. Math. Comput. **75**, 1659–1674 (2006)
31. Martin, V., Jaffré, J., Roberts, J.E.: Modeling fractures and barriers as interfaces for flow in porous media. SIAM J. Sci. Comput. **26**, 1667–1691 (2005)
32. Moortgat, J., Sun, S., Firoozabadi, A.: Compositional modeling of three-phase flow with gravity using higher-order finite element methods. Water Resour. Res. **47**, W05511 (2011)
33. Noorishad, J., Mehran, M.: An upstream finite element method for solution of transient transport equation in fractured porous media. Water Resour. Res. **18**, 588–596 (1982)
34. Pruess, K., Narasimhan, T.: A practical method for modeling fluid and heat flow in fractured porous media. SPE J. **25**, 14–26 (1985)

35. Scott, R., Zhang, S.: Finite element interpolation of nonsmooth functions satisfying boundary conditions. Math. Comput. **54**, 483–493 (1990)
36. Song, P., Sun, S.: Contaminant flow and transport simulation in cracked porous media using locally conservative schemes. Adv. Appl. Math. Mech. **4**, 389–421 (2012)
37. Stevenson, R.: Optimality of a standard adaptive finite element method. Found. Comput. Math. **2**, 245–269 (2007)
38. Sun, S., Wheeler, M.F.: Symmetric and nonsymmetric discontinuous Galerkin methods for reactive transport in porous media. SIAM J. Numer. Anal. **43**, 195–219 (2005)
39. Sun, S., Wheeler, M.F.: L2(H1) norm a posteriori error estimation for discontinuous Galerkin approximations of reactive transport problems. J. Sci. Comput. **22**, 501–530 (2005)
40. Tang, T., Xu, J.: Adaptive Computations: Theory and Algorithms. Science Press, Beijing (2007)
41. Verfürth, R.: A posteriori error estimates and adaptive mesh-refinement techniques. J. Comput. Appl. Math. **50**, 67–83 (1994)
42. Verfürth, R.: A Review of A Posteriori Error Estimation and Adaptive Mesh-Refinement Techniques. Wiley-Teubner, Chichester (1996)
43. Warren, J., Root, P.: The behavior of naturally fractured reservoirs. SPE J. **3**, 245–255 (1963)
44. Wu, Y.S., Pruess, K.: A multiple-porosity method for simulation of naturally fractured petroleum reservoirs. SPE Reserv. Eng. **3**, 327–336 (1988)
45. Zidane, A., Firoozabadi, A.: An efficient numerical model for multicomponent compressible flow in fractured porous media. Adv. Water Resour. **74**, 127–147 (2014)